

## Comparative Study of AUSM-Family Schemes in Compressible Multiphase Flow Simulations

K. Kitamura\*\* and M.-S. Liou\*

Corresponding author: kitamura.keiichi@jaxa.jp

\* NASA Glenn Research Center, USA

\*\* JAXA JEDI Center, Japan.

**Abstract:** Several recently-developed AUSM-family numerical flux functions have been successfully extended to compressible multifluid and multiphase flow computations, based on stratified flow model concept, following the work by M.-S. Liou, C.-H. Chang, L. Nguyen, and T.G. Theofanous [AIAA J. 46:2345-2356, 2008]. Through an extensive survey by comparing flux functions of different amounts of dissipation as well as physical modeling parameters, the following are found: (1) AUSM<sup>+</sup>-up with large dissipation parameters for low speeds ( $K_p=K_u=1$ ), that with small dissipation ( $K_p=K_u=0.5$ ), SLAU2, or AUSM<sup>+</sup>-up2 ( $K_p=1$ ) can be used for all the problems solved here, even for a challenging 2D shock/water-droplet interaction, with this order of smoothness/diffusivity of solutions; (2) SLAU showed oscillatory behaviors [though not as catastrophic as those of AUSM<sup>+</sup> - a special case of AUSM<sup>+</sup>-up with  $K_p=K_u=0$ ] due to insufficient dissipation arising from inherent limitation in extension of its dissipation term; (3) AUSM<sup>+</sup>-up modified by Y.-Y. Niu, Y.-C. Lin, and C.-H. Chang [Int. J. Numer. Meth. Fluids, 58:879-896, 2008] and AUSMPW+ are applicable to limited, two-phase flow problems without steep pressure gradients, within the current two-fluid framework.

*Keywords:* Multiphase Flow, Computational Fluid Dynamics, Numerical Algorithms, AUSM-Family, Two-Fluid Model, Stratified Flow Model.

## 1 Introduction

Multifluid and multiphase flow computations have been attracting many researchers and practitioners over wide-ranging fields of study for several decades [1-20]. Some recent studies have been dedicated to extend incompressible flow methods to compressible flows, because compressible methods obviously have more applicability, for instance, as in [5]. As a result, while we have many approaches for multiphase flows with their own pros and cons, it is difficult for users or beginner researchers to choose appropriate methods to meet their demands (see Figure 1). Those methods are categorized into two major groups, i.e., interface sharpening method and interface capturing method. The former method employs an additional step to recognize the location of interface and impose a numerically-smoothed representation of jumps across the interface. The latter, on the other hand, captures interface discontinuities as part of numerical solution, but the jumps are smeared over a number of mesh points, largely depending on the numerical flux functions and order of accuracy in discretization. Because of not using “tracking” devices, the interface capturing approach is “the most practical approach” for dealing with complex geometries like turbopumps, as stated in [21], and also it is able to deal with

dynamic creation of cavitation [16]. Among the latter group, we chose the so-called two-fluid modeling (or also known as effective-fluid-modeling, EFM), which allows each fluid to possess its own physical variables except for pressure, whereas its one-fluid counterpart deals with averaged (mixture) density and other common variables, causing difficulties in its own justification under some circumstances [11].

A novel approach of two-fluid modeling was proposed by Liou et al. [14] based on the stratified flow model concept [13, 22], in which AUSM<sup>+</sup>-up [23] flux function, one of AUSM-family schemes [23-27], was successfully extended from the single-phase version without relying upon an expensive, exact Riemann solver [13]. AUSM-family fluxes are known to give robust and accurate solutions efficiently in single-phase gas flows from low speed to hypersonic, but they have not fully been surveyed in multiphase flows. In addition, some issues were left open in [14], such as built-in parameters of the flux function.

Thus, as the first step of exploring a better option of methods and parameters, we will extend the recently-developed flux functions of AUSM-family [25-27] and compare their performances in multifluid and multiphase flows. The results and discoveries herein will provide users with guidelines on choosing methods, and also give us both directions and motivations for further developments of numerical modeling of multiphase flows.

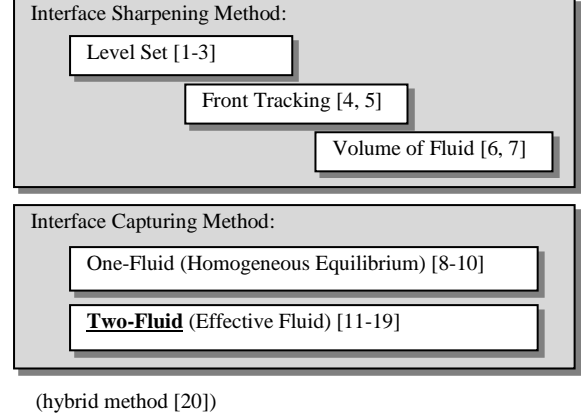


Figure 1: Various Methods for Multiphase Flow Computations.

## 2 Numerical Methods

### 2.1 Two-Fluid Modeling (or Effective-Fluid-Modeling, EFM)

The 2-D compressible Euler equations in two-fluid modeling (or effective-fluid-modeling, EFM) are written as:

$$\frac{\partial \mathbf{Q}_k}{\partial t} + \frac{\partial \mathbf{E}_k}{\partial x} + \frac{\partial \mathbf{F}_k}{\partial y} = \mathbf{P}_k^{\text{int}} + \mathbf{S}_k, \quad k=1, 2 \quad (1a)$$

$$\mathbf{Q}_k = \begin{bmatrix} \alpha \rho \\ \alpha \rho u \\ \alpha \rho v \\ \alpha \rho E \end{bmatrix}_k, \mathbf{E}_k = \begin{bmatrix} \alpha \rho u \\ \alpha \rho u^2 + \alpha p \\ \alpha \rho uv \\ \alpha \rho uH \end{bmatrix}_k, \mathbf{F}_k = \begin{bmatrix} \alpha \rho v \\ \alpha \rho vu \\ \alpha \rho v^2 + \alpha p \\ \alpha \rho vH \end{bmatrix}_k, \mathbf{P}_k^{\text{int}} = \begin{bmatrix} 0 \\ p^{\text{int}} \frac{\partial \alpha}{\partial x} \\ p^{\text{int}} \frac{\partial \alpha}{\partial y} \\ -p^{\text{int}} \frac{\partial \alpha}{\partial t} \end{bmatrix}_k, \mathbf{S}_k = \begin{bmatrix} 0 \\ \alpha \rho g_x \\ \alpha \rho g_y \\ \alpha \rho g_x u + \alpha \rho g_y v \end{bmatrix}_k \quad (1b)$$

$$\alpha_g + \alpha_l = 1 \quad (2)$$

$$p_g = p_l \equiv p \quad (3)$$

$$p_g^{\text{int}} = p_l^{\text{int}} \equiv p^{\text{int}} \quad (4)$$

$$p^{\text{int}} = p - \delta p^* \quad (5)$$

where  $\alpha$  is volume fraction,  $\rho$  is density,  $u, v$  are velocity components in Cartesian coordinates,  $E$  is total energy [ $E = e + (p/\rho)$ ,  $e$  is internal energy],  $p$  is pressure,  $H$  is total enthalpy [ $H = E + (p/\rho)$ ], and  $g_x$  and  $g_y$  are projection of gravity constant,  $9.8 \text{ m/s}^2$ , to  $x$  and  $y$  coordinates, respectively, used only in ‘Faucet’ problem in 3.2. Since we treat only gas-liquid systems in this study,  $k=1, 2$  is interchangeable with  $k=g, l$ , where  $g$  stands for gas and  $l$  is liquid. As in single-fluid equations,  $\mathbf{Q}$  is conservative vector,  $\mathbf{E}, \mathbf{F}$  are inviscid flux vectors in  $x, y$  directions, respectively, but with  $\alpha$  included;  $\mathbf{P}_k^{\text{int}}$  is the so-called interfacial pressure, and  $\mathbf{S}_k$  is the source term containing gravity force considered in the ‘Faucet’ problem in this study. The Eq. (2) expresses the compatibility relation for volume fractions, Eq. (3) and Eq. (4) assume pressure equilibrium, and Eq. (5) gives interfacial pressure,  $p^{\text{int}}$ , as a departure from  $p$  by  $\delta p^*$ , which will be explained further in 2.3. Now we have 14 unknowns [ $\alpha, \rho, u, v, e, p, p^{\text{int}}$ ] $_k$  closed by 12 equations [Eqs. (1)-(5)] with two equations-of-state (EOS) described later in 2.4.

## 2.2 Stratified Flow Model and Discretization

Within the framework of a finite-volume, shock-capturing method, we follow the concept of stratified flow model proposed first by Stewart and Wendroff [22] (Fig. 2a) which was later refined by Chang and Liou [13] and Liou et al. [14]. In this model, the interfacial pressure  $p^{\text{int}}$  must work within the cell only, and the volume fractions are assumed to be continuous within the cell but allowed a jump at the cell boundaries (Fig. 2b). The discretized form of Eq. (1), by retaining only 1D form for illustration, is:

$$\frac{V_j}{\Delta t} \Delta \mathbf{Q}_j + \mathbf{E}_{j+1/2} S_{j+1/2} - \mathbf{E}_{j-1/2} S_{j-1/2} = p_j^{\text{int}} \begin{bmatrix} 0 \\ \alpha_{j+1/2,L} - \alpha_{j-1/2,R} \\ \frac{V_j(\alpha_j^{n+1} - \alpha_j^n)}{\Delta t} \end{bmatrix} + \mathbf{S}_j \quad (6)$$

where subscript  $k$  is omitted, and  $j$  applies to each direction in 2D,  $V_j$  is volume of cell  $j$ ,  $S_{j+1/2}$  is area of the cell interface between cells  $j$  and  $j+1$ . Cell interfacial variables such as  $\alpha_{j+1/2,L}$  are given by spatially 2nd-order accurate MUSCL interpolation [28] with Van Albada’s limiter [29] (limiter coefficient is set as  $10^{-20}$ ; limiter effects was surveyed as in Appendix A). Note that the present method is valid only for the 2nd-order or higher accuracy, because the 1st-order reconstruction yields to  $\alpha_{j+1/2,L} = \alpha_{j-1/2,R} = \alpha_j$  (i.e., no interfacial pressure acting within a cell). Three-stage, 3rd-order TVD Runge-Kutta method [30] is used for time integration, and its details will be explained later in 2.6. The numerical code is extended from a single-fluid version previously used by Kitamura et al. in [31].

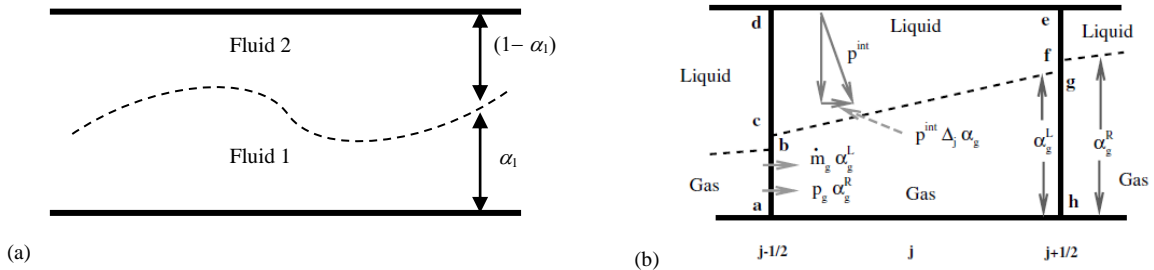


Figure 2: Illustrations of Stratified Flow Concept, (a) Generic; (b) One-dimensional, Discretized [14].

## 2.3 Interfacial Pressure

The interfacial pressure,  $p^{\text{int}}$ , introduced by Stuhmiller [32], working at a phase interface *within* a cell according to Liou et al. [14], is as already given as:

$$p^{\text{int}} = p - \delta p^* \quad (5)$$

and for a gas-liquid system,  $\delta p^*$  is usually given by

$$\delta p^* = \sigma \frac{\alpha_g \alpha_l \rho_g \rho_l}{\alpha_g \rho_l + \alpha_l \rho_g} |\mathbf{u}_l - \mathbf{u}_g|^2 \quad (7)$$

or more simply, after assuming  $\rho_l \gg \rho_g$  and  $(\alpha_l, \alpha_g)$  being finite,

$$\delta p^* = C_p^* \alpha_l \rho_g |\mathbf{u}_l - \mathbf{u}_g|^2 \quad (8)$$

The interfacial pressure coefficient,  $C_p^*$  or  $\sigma$ , should be large enough (at least larger than or equal to unity) to keep the system hyperbolic [14, 19]. We will make use of Eq. (8) with  $C_p^*=2.0$ , although there is still an open discussion of how big or small this value should be [14]:

Furthermore, in order to prevent  $p^{\text{int}}$  from deviating too much from the static pressure  $p$ , the following limitation is imposed so that  $\delta p^*$  does not exceed a fraction of  $p$ :

$$\delta p^* = \min(\delta p^*, \varepsilon_p p) \quad (9)$$

where  $\varepsilon_p = 0.01$  is used as in [13] for all the numerical tests here.

## 2.4 Equation of State (EOS)

For closure of the system we adopted the stiffened-gas model proposed by Harlow and Amsden [33] as an equation of state (EOS) expressed as:

$$p_k = \rho_k \frac{\gamma_k - 1}{\gamma_k} C_{pk} T_k - p_{k\infty} \quad (10a)$$

$$e_k = \frac{C_{pk}}{\gamma_k} T_k + \frac{p_{k\infty}}{\rho_k} \quad (10b)$$

$$a_k = \left( \frac{\gamma_k (p_k + p_{k\infty})}{\rho_k} \right)^{1/2} \quad (10c)$$

where  $e_k$  is the internal energy per unit mass of fluid  $k$ ,  $a_k$  is the speed of sound, with the following values [14]:

$$\gamma_g = 1.4, C_{pg} = 1004.5 \text{ J/(kg K)}, p_{g\infty} = 0 \text{ Pa} \quad \text{for gas} \quad (11a)$$

$$\gamma_l = 2.8, C_{pl} = 4186 \text{ J/(kg K)}, p_{l\infty} = 8.5 \times 10^8 \text{ Pa} \quad \text{for liquid} \quad (11b)$$

that is to say, the (ideal) gas is treated as merely a special case of the same EOS.

## 2.5 Numerical Fluxes

An AUSM-family flux function of AUSM<sup>+</sup>-up [23], SLAU [25], SLAU2 [26], AUSM<sup>+</sup>-up2 [27], AUSM<sup>+</sup>-up with Niu et al. modification [17], or AUSMPW+ [34] is used to calculate inviscid numerical fluxes at cell-interfaces for each phase, denoted as  $\mathbf{F}_{k,1/2,L/R}$ , where “L” and “R” stands for left and right cells, respectively. The numerical flux is commonly expressed as:

$$\mathbf{F}_{k,1/2,L/R} = \frac{\dot{m}_{k,1/2} + |\dot{m}_{k,1/2}|}{2} \Psi_{k,L} + \frac{\dot{m}_{k,1/2} - |\dot{m}_{k,1/2}|}{2} \Psi_{k,R} + \alpha_{k,1/2,L/R} \tilde{P}_{k,1/2} \mathbf{N} \quad (12a)$$

$$\Psi_k = (\alpha, \alpha u, \alpha v, \alpha H)_k^T, \quad \mathbf{N} = (0, n_x, n_y, 0)^T \quad (12b)$$

Be aware that different void fractions exist to the left and right of an interface, and the last term in (12a) will contribute differently, i.e., different numerical fluxes  $\mathbf{F}_{k,1/2,L}$  and  $\mathbf{F}_{k,1/2,R}$ , to the left and right cells respectively. In the case of single-phase flux, it becomes common to both sides and is a special case of the above formula, because void fraction is constant. These schemes [23, 25-27, 34] have showed satisfactory performance in single-phase gas flows from low speed to hypersonic, but have not been fully surveyed in multiphase flows yet. Here we describe multiphase flow versions of those fluxes extended as in [14].

### 2.5.1 AUSM<sup>+</sup>-up

First, AUSM<sup>+</sup>-up by Liou [23] for multiphase flows [14] is briefly reviewed as follows. The mass flux is given by

$$\dot{m}_{k,1/2} = M_{k,1/2} a_{1/2} \begin{cases} \rho_{k,L} & \text{if } M_{k,1/2} > 0 \\ \rho_{k,R} & \text{otherwise} \end{cases} \quad (13a)$$

$$M_{k,1/2} = M_{(4)k}^+(M_{k,L})_{|1/8} + M_{(4)k}^-(M_{k,R})_{|1/8} + M_{pk} \quad (13b)$$

$$M_{(4)}^\pm(M)_{|1/8} = \begin{cases} \frac{1}{2}(M \pm |M|), & \text{if } |M| \geq 1 \\ \pm \frac{1}{4}(M \pm 1)^2 \pm \frac{1}{8}(M^2 - 1)^2, & \text{otherwise} \end{cases} \quad (13c)$$

$$M_{pk} = -\frac{K_p}{f_a} \max(1 - \bar{M}_k^2, 0) \frac{p_R - p_L}{\bar{\rho}_k a_{1/2}^2}, \quad \bar{\rho}_k = \frac{\rho_{k,L} + \rho_{k,R}}{2} \quad (13d)$$

$$M_k = \frac{V_{k,n}}{a_{1/2}} = \frac{u_k n_x + v_k n_y}{a_{1/2}} \quad (13e)$$

$$\bar{M}_k^2 = \frac{V_{k,n}^{+2} + V_{k,n}^{-2}}{2a_{1/2}^2} \quad (13f)$$

where  $f_a = 1$  here (hence, no prescribed Mach number is used), and the speed of sound,  $a_{1/2}$ , common to gas and liquid [14], is

$$a_{1/2} = \frac{1}{2}(a_{l,1/2} + a_{g,1/2}) \quad (13g)$$

$$a_{k,1/2} = \bar{a}_k = \frac{a_{k,L} + a_{k,R}}{2} \quad (13h)$$

where arithmetic mean of left and right states is used for the speed of sound for each fluid,  $a_{1/2,k}$ . Although it is argued that this value can be obtained differently, e.g., geometric mean of left and right states, the effect of choosing  $a_{1/2}$  is not discussed here. However, we confirmed that the present choice gives robust performances to all the fluxes used here, in general.

Then, the pressure flux is

$$\tilde{p}_{k,1/2} = P_{(5)k}^+(M_{k,L})_{|3/16} p_L + P_{(5)k}^-(M_{k,R})_{|3/16} p_R + p_{uk} \quad (13i)$$

$$P_{(5)}^\pm(M)_{|3/16} = \begin{cases} \frac{1}{2}(1 \pm \text{sign}(M)), & \text{if } |M| \geq 1 \\ \frac{1}{4}(M \pm 1)^2 (2 \mp M) \pm \frac{3}{16} M (M^2 - 1)^2, & \text{otherwise} \end{cases} \quad (13j)$$

$$p_{uk} = -K_u P_{(5)k}^+(M_{k,L})_{|3/16} P_{(5)k}^-(M_{k,R})_{|3/16} \bar{\rho}_k f_a a_{1/2} (V_{k,n}^- - V_{k,n}^+) \quad (13k)$$

where tunable parameters are  $K_p$  and  $K_u$ , both set as unity in the previous works [13, 14, 18].

As seen above, the differences from single-phase version in [23] are (1) separate fluxes but common speed of sound for gas and liquid; (2) scaling function  $f_a$  is eliminated, and hence, no cutoff or freestream Mach number is required, because we are dealing with transient flows only; (3) averaged

density, rather than summation of left and right densities, is used in Eq. (13k), thus, there would be equivalently a factor of 2 difference in  $K_u$ , i.e., setting a value of  $K_u$  is equivalent to setting a half of it in [23]. In this work, AUSM<sup>+</sup>-up with different  $K_p$  and  $K_u$  will be simply denoted as AUSM<sup>+</sup>-up ( $K_p, K_u$ ). Note that AUSM<sup>+</sup>-up (1, 1) is commonly used choice, and that AUSM<sup>+</sup>-up (0, 0) corresponds to AUSM<sup>+</sup> [24], the version prior to AUSM<sup>+</sup>-up, having no low speed treatment. In this study, different coefficients ( $K_p, K_u$ ) = (1, 1), (0.5, 0.5), and (0, 0) are selected for comparison.

### 2.5.2 SLAU

SLAU (Simple Low-dissipation AUSM) by Shima and Kitamura [25] is also extended for multiphase flows in the same manner as in AUSM<sup>+</sup>-up. The mass flux for each fluid is given as:

$$\dot{m}_{k,1/2} = \frac{1}{2} \left\{ \rho_{k,L} \left( V_{k,nL} + |\bar{V}_{k,n}|^+ \right) + \rho_{k,R} \left( V_{k,nR} - |\bar{V}_{k,n}|^- \right) - \frac{\chi_k}{a_{1/2}} (p_R - p_L) \right\} \quad (14a)$$

$$|\bar{V}_{k,n}|^+ = (1 - g_k) |\bar{V}_{k,n}| + g_k |V_{k,nL}|, \quad |\bar{V}_{k,n}|^- = (1 - g_k) |\bar{V}_{k,n}| + g_k |V_{k,nR}| \quad (14b)$$

$$|\bar{V}_{k,n}| = \frac{\rho_{k,L} |V_{k,nL}| + \rho_{k,R} |V_{k,nR}|}{\rho_{k,L} + \rho_{k,R}} \quad (14c)$$

$$g_k = -\max[\min(M_{k,L}, 0), -1] \cdot \min[\max(M_{k,R}, 0), 1] \in [0, 1] \quad (14d)$$

$$\chi_k = (1 - \hat{M}_k)^2 \quad (14e)$$

$$\hat{M}_k = \min \left( 1.0, \frac{1}{a_{1/2}} \sqrt{\frac{\mathbf{u}_{k,L}^2 + \mathbf{u}_{k,R}^2}{2}} \right) \quad (14f)$$

$$M_k = \frac{V_{k,n}}{a_{1/2}} = \frac{u_k n_x + v_k n_y}{a_{1/2}} \quad (14g)$$

where the common speed of sound for gas and liquid  $a_{1/2}$  is given again by

$$a_{1/2} = \frac{1}{2} (a_{l,1/2} + a_{g,1/2}) \quad (13g)$$

$$a_{k,1/2} = \bar{a}_k = \frac{a_{k,L} + a_{k,R}}{2} \quad (13h)$$

and the pressure flux is

$$\tilde{p}_{k,1/2} = \frac{p_L + p_R}{2} + \frac{P_{(5)k}^+(M_{k,L})|_0 - P_{(5)k}^-(M_{k,R})|_0}{2} (p_L - p_R) \quad (14h)$$

$$+ (1 - \chi_k) \left( P_{(5)k}^+(M_{k,L})|_0 + P_{(5)k}^-(M_{k,R})|_0 - 1 \right) \frac{p_L + p_R}{2} \quad (14i)$$

$$P_{(5)}^\pm(M)|_0 = \begin{cases} \frac{1}{2} (1 \pm \text{sign}(M)), & \text{if } |M| \geq 1 \\ \frac{1}{4} (M \pm 1)^2 (2 \mp M), & \text{otherwise} \end{cases}$$

The dissipation term (last term) in pressure flux had been originally designed only for an ideal gas, according to the relation  $\bar{p} \propto \bar{\rho} \bar{a}^2$ . This term was then modified later in SLAU2 so that real fluids are treated in a unified manner.

### 2.5.3 SLAU2 and AUSM<sup>+</sup>-up2

In SLAU2 [26], the dissipation term in pressure flux of SLAU [Eq. (14i)] is modified as:

$$\begin{aligned}\tilde{p}_{k,1/2} = & \frac{p_L + p_R}{2} + \frac{P_{(5)k}^+(M_{k,L})|_0 - P_{(5)k}^-(M_{k,R})|_0}{2} (p_L - p_R) \\ & + \sqrt{\frac{\mathbf{u}_{k,L}^2 + \mathbf{u}_{k,R}^2}{2}} \left( P_{(5)k}^+(M_{k,L})|_0 + P_{(5)k}^-(M_{k,R})|_0 - 1 \right) \bar{\rho}_k a_{1/2}\end{aligned}\quad (15)$$

for (1) readily extension to real fluids and (2)  $\gamma$  times dissipation addition at subsonic and more to stronger shocks.

If the pressure flux of AUSM<sup>+</sup>-up in Eqs. (13i-k) are replaced with Eq. (15), AUSM<sup>+</sup>-up2 [27] is realized (in this study,  $K_p = 1$  is chosen). In both flux functions, arithmetic mean of left and right states is employed for speed of sound of each fluid [Eq. (14h)]. Then, arithmetic mean of gas and liquid phases is used as a common speed of sound [Eq. (13g)], as in AUSM<sup>+</sup>-up and SLAU.

#### 2.5.4 AUSM<sup>+</sup>-up (Niu)

Niu et al. [17] proposed a modified version of AUSM<sup>+</sup>-up, by replacing the dissipation term of mass flux [Eq. (14d)] with:

$$M_{pk} = -\frac{\rho_{k,L}\rho_{k,R}}{p_L\rho_{k,R} + p_R\rho_{k,L}} \Delta M_k \cdot \max\left(1 - \text{int}(\bar{M}_k^2), 0\right) \frac{p_R - p_L}{\bar{\rho}_k a_{1/2}} \quad (16a)$$

$$\Delta M_k = M_{(4)}^+(M_L) - M_{(1)}^+(M_L) - M_{(4)}^-(M_R) + M_{(1)}^-(M_R) \quad (16b)$$

with additional changes:

$$M_{k,1/2} = M_{(1)k}^+(M_{k,L}) + M_{(1)k}^-(M_{k,R}) \quad (16c)$$

$$M_{(i)}^\pm(M) = \frac{1}{2}(M \pm |M|) \quad (16d)$$

Note that this modification eliminated one user-specified parameter,  $K_p = 1$ , albeit its dimension is altered, too [Eq. (13d) had no dimension, but Eq. (16a) has dimension of inverse of velocity, s/m]; hence, leading to problem-dependent amount of dissipation.

#### 2.5.5 AUSMPW+

Kim et al. [34] proposed AUSMPW+, featuring pressure-based weight functions with multidimensional dissipation. Instead of Eq. (12a), it is expressed as:

$$\mathbf{F}_{k,1/2,L/R} = \bar{M}_{k,L}^+ a_{1/2} \Psi_{k,L} + \bar{M}_{k,R}^- a_{1/2} \Psi_{k,R} + \alpha_{k,1/2,L/R} \tilde{p}_{k,1/2} \mathbf{N} \quad (17a)$$

where

For  $M_{k,1/2} \geq 0$ ,

$$\bar{M}_{k,L}^+ = M_{k,L}^+ + M_{k,R}^- \cdot \left[ (1-w) \cdot (1+f_R) - f_L \right] \quad (17b)$$

$$\bar{M}_{k,R}^- = M_{k,R}^- \cdot w \cdot (1+f_R)$$

For  $M_{k,1/2} < 0$ ,

$$\bar{M}_{k,L}^+ = M_{k,L}^+ \cdot w \cdot (1+f_L) \quad (17c)$$

$$\bar{M}_{k,R}^- = M_{k,R}^- + M_{k,L}^+ \cdot \left[ (1-w) \cdot (1+f_L) - f_R \right]$$

The pressure-based weighting functions are given by:

$$w = 1 - \Pi_{1/2}^3, \quad \Pi_{1/2} = \min\left(\frac{p_L}{p_R}, \frac{p_R}{p_L}\right) \quad (17d)$$

$$f_{L,R} = \begin{cases} \left( \frac{p_{L,R} - 1}{p_s} \right) \cdot \min \left( 1, \frac{\min(p_{L,1}, p_{R,1}, p_{L,2}, p_{R,2})}{\min(p_L, p_R)} \right)^2 & \text{if } p_s \neq 0 \\ 0 & \text{if } p_s = 0 \end{cases} \quad (17e)$$

$$p_s = P_L^+ p_L + P_R^- p_R \quad (17f)$$

where  $p_{L,1}$  and  $p_{L,2}$ , and  $p_{R,1}$  and  $p_{R,2}$  are pressure at neighbor cells of ‘‘L’’ and ‘‘R,’’ respectively, in the other direction to the cell-interface between ‘‘L’’ and ‘‘R’’ in 2D.

Then, the mass flux is written as:

$$M_{k,1/2} = M_{(4)k}^+ (M_{k,L})_0 + M_{(4)k}^- (M_{k,R})_0 \quad (17g)$$

$$M_{(4)k}^\pm (M)_0 = \begin{cases} \frac{1}{2} (M \pm |M|), & \text{if } |M| \geq 1 \\ \pm \frac{1}{4} (M \pm 1)^2, & \text{otherwise} \end{cases} \quad (17h)$$

and the pressure flux is:

$$\tilde{P}_{k,1/2} = P_{(5)k}^+ (M_{k,L})_0 p_L + P_{(5)k}^- (M_{k,R})_0 p_R \quad (17i)$$

$$P_{(5)k}^\pm (M)_0 = \begin{cases} \frac{1}{2} (1 \pm \text{sign}(M)), & \text{if } |M| \geq 1 \\ \frac{1}{4} (M \pm 1)^2 (2 \mp M), & \text{otherwise} \end{cases} \quad (17j)$$

The speed of sound for each phase is defined using cell-interface-normal component of the total enthalpy for this flux:

$$a_{k,1/2} = \begin{cases} a_{k,s}^2 / \max(|V_{k,nL}|, a_{k,s}), & \text{if } V_{k,nL} + V_{k,nR} \geq 0 \\ a_{k,s}^2 / \max(|V_{k,nR}|, a_{k,s}), & \text{if } V_{k,nL} + V_{k,nR} < 0 \end{cases} \quad (17k)$$

$$a_{k,s} = \sqrt{2H_{k,n}(\gamma_k - 1)/(\gamma_k + 1)} \quad (17l)$$

$$H_{k,n} = \frac{1}{2} \left( H_{k,L} - \frac{V_{k,L}^2}{2} + H_{k,R} - \frac{V_{k,R}^2}{2} \right) \quad (17m)$$

where the subscript  $n$  denotes the normal component, and the  $t$  is the tangential. Then, the gas and liquid speed of sound are averaged arithmetically as the final value:

$$a_{1/2} = \frac{1}{2} (a_{t,1/2} + a_{g,1/2}) \quad (13g)$$

Further modifications were made by Kim and Ihm in [10] for one-fluid, two-phase flow extension with some success. However, since their modifications involve many mixture variables (e.g. mixture density) that are absent in two-fluid modeling, we took its original form for each phase here.

## 2.6 Time Integration, Decoding, and Update of Variables

Equation (6) is rewritten in the three-stage TVD Runge-Kutta [30] form as:

$$\hat{\mathbf{Q}}_j^{(1)} = \hat{\mathbf{Q}}_j^n + \frac{\Delta t}{V_j} \mathbf{R}_j^n \quad (18a)$$

$$\hat{\mathbf{Q}}_j^{(2)} = \frac{3}{4} \hat{\mathbf{Q}}_j^n + \frac{1}{4} \hat{\mathbf{Q}}_j^{(1)} + \frac{1}{4} \frac{\Delta t}{V_j} \mathbf{R}_j^{(1)} \quad (18b)$$

$$\hat{\mathbf{Q}}_j^{n+1} = \frac{1}{3} \hat{\mathbf{Q}}_j^n + \frac{2}{3} \hat{\mathbf{Q}}_j^{(2)} + \frac{2}{3} \frac{\Delta t}{V_j} \mathbf{R}_j^{(2)} \quad (18c)$$

$$\hat{\mathbf{Q}}_j \equiv \mathbf{Q}_j + \begin{bmatrix} 0 \\ 0 \\ p_j^{\text{int}} \alpha_j \end{bmatrix} = \begin{bmatrix} \hat{Q}_1 \\ \hat{Q}_2 \\ \hat{Q}_3 \end{bmatrix} \quad (18d)$$

$$\mathbf{R}_j \equiv -[\mathbf{E}_{j+1/2} \mathbf{S}_{j+1/2} - \mathbf{E}_{j-1/2} \mathbf{S}_{j-1/2}] + \begin{bmatrix} 0 \\ p_j^{\text{int}} (\alpha_{j+1/2,L} - \alpha_{j-1/2,R}) \\ 0 \end{bmatrix} + \mathbf{S}_j \quad (18e)$$

where  $k$  is omitted, and the term  $(p^{\text{int}} \alpha)$  is included in  $\hat{\mathbf{Q}}$  as in Eq. (18d) [14 ,17], but  $p^{\text{int}}$  is frozen at  $n$ -th time step value throughout the Runge-Kutta stages [17].

Once  $\hat{\mathbf{Q}}^{n+1}$  is obtained, the following decoding process is required to update  $p^{n+1}$  and  $\alpha_k^{n+1}$ :

$$p = \frac{1}{2} \left( B + \sqrt{B^2 + 4C} \right) \quad (19a)$$

$$\alpha_k = \frac{\hat{A}_k}{p + \hat{a}_k} \quad (19b)$$

with

$$\hat{A}_k = (\gamma_k - 1) \left( \hat{Q}_{3,k} - \frac{\hat{Q}_{2,k}^2}{2\hat{Q}_{1,k}} \right) \quad (19c)$$

$$B = \sum_{k=1}^2 (\hat{A}_k - \hat{a}_k) \quad (19d)$$

$$C = \hat{a}_1 \hat{A}_2 + \hat{a}_2 \hat{A}_1 - \hat{a}_1 \hat{a}_2 \quad (19e)$$

$$\hat{a}_k = \gamma_k p_{k,\infty} + (\gamma_k - 1) p^{\text{int}} \quad (19f)$$

because the pressure is the positive root of the following equation.

$$F(p) = p^2 - Bp - C = 0 \quad (20)$$

Since huge values such as  $p_{l\infty}$  are handled in Eqs. (18)-(19), the resultant numerical errors are also large. Thus, the simultaneous Newton iteration method is introduced to improve accuracy for Eq. (19b) [13] as:

$$\begin{cases} F_g = (p + \hat{a}_g) \alpha_g - \hat{A}_g = 0 \\ F_l = (p + \hat{a}_l) \alpha_l - \hat{A}_l = 0 \end{cases} \quad (21)$$

Usually, a few iterations are enough to drive pressure error under  $O(10^{-5})$ .

Then, following Paillère et al. [15] and Chang and Liou [17], variables of “vanishing” phase (i.e.,  $\varepsilon_{\min} \leq \alpha_1 \leq \varepsilon_{\max}$ ) are blended with those of remaining phase (i.e.,  $\alpha_2 \approx 1$ ) to enhance stability:

$$(q_1)_{\text{adjust}} = G(\xi_1) q_1 + (1 - G(\xi_1)) q_2, \quad q = \mathbf{u}, T \quad (22a)$$

$$G(\xi_1) = -\xi_1^2 (2\xi_1 - 3) \quad (22b)$$

$$\xi_1 = \frac{\alpha_1 - \varepsilon_{\min}}{\varepsilon_{\max} - \varepsilon_{\min}} \quad (22c)$$

where  $G$  is a smooth function satisfying  $G(0) = 0$ ,  $G(1) = 1$ , and  $G'(0) = G'(1) = 0$ . The small values of  $\varepsilon_{\min}$  and  $\varepsilon_{\max}$  are chosen as  $0.1 \varepsilon (=10^{-8})$  and  $10^3 \varepsilon (=10^{-4})$  in this paper, if not mentioned otherwise. If  $\alpha_1$  is below  $\varepsilon_{\min}$ ,  $\alpha_1 = \varepsilon_{\min}$  is enforced. Here  $k = 1, 2$  is interchangeable with  $k = g, l$  and  $k = l, g$  both. We must update  $(\mathbf{u}, T)$ , not  $(\mathbf{u}, \rho)$ . If the density is replaced by that of the other phase, which is  $O(10^3)$  different, the temperature may have huge error, say,  $O(10^5)$  [K] of water in the standard air condition,

for instance.

## 2.7 Boundary Conditions

Since a cell-centered, 2D structured grid solver is used here, the following typical boundary conditions using the typical “ghost cell” approach are applied as in [15]:

- Inlet: all the variables are imposed except for pressure, which is extrapolated from the interior cell.
- Outlet: only pressure is imposed, and all the other variables are extrapolated from the interior cell.
- Side (for a 1D problem): all the variables are extrapolated from the interior cell (for the direction irrelevant to the problem to be solved).
- Slip: also known as “mirror” condition in which the opposite sign is put to the velocity component normal to the boundary, and all the other variables are extrapolated from the interior cell.

## 3 Numerical Examples

In what follows, we shall demonstrate that recently-developed AUSM-family fluxes, i.e., AUSM<sup>+</sup>-up (1, 1), AUSM<sup>+</sup>-up (0.5, 0.5), AUSM<sup>+</sup>-up (0, 0), SLAU, SLAU2, AUSM<sup>+</sup>-up2, AUSM<sup>+</sup>-up (Niu), and AUSMPW+ are extended to multifluid and multiphase flows in the same framework, as well as comparisons of their performances. Here, as explained in detail by Saurel and Abgrall [16], the term (numerical) “multifluid flow” stands for a flow in which each computational cell is filled with a (nearly) pure fluid (either gas or liquid) except for well-defined phase interfaces, whereas the “multiphase flow” allows the cells to contain some portions of both phases with many interfaces treated in an averaged manner, e.g., 80% water and 20% air as in the ‘Faucet’ problem.

For convenience, the following “CFL-like number,” usually taken between 0.1 and 0.63, is used to describe how big the time step is:

$$CFL = \Delta t / \min_j \left( \frac{\Delta x}{\max(a_g, a_l) + \max(|\mathbf{u}_g|, |\mathbf{u}_l|)} \right)_j \quad (23)$$

For ease of reference, all the results will be summarized in Table 1 at the bottom of this section.

### 3.1 Moving Phase Discontinuity (Two-Fluid Flow)

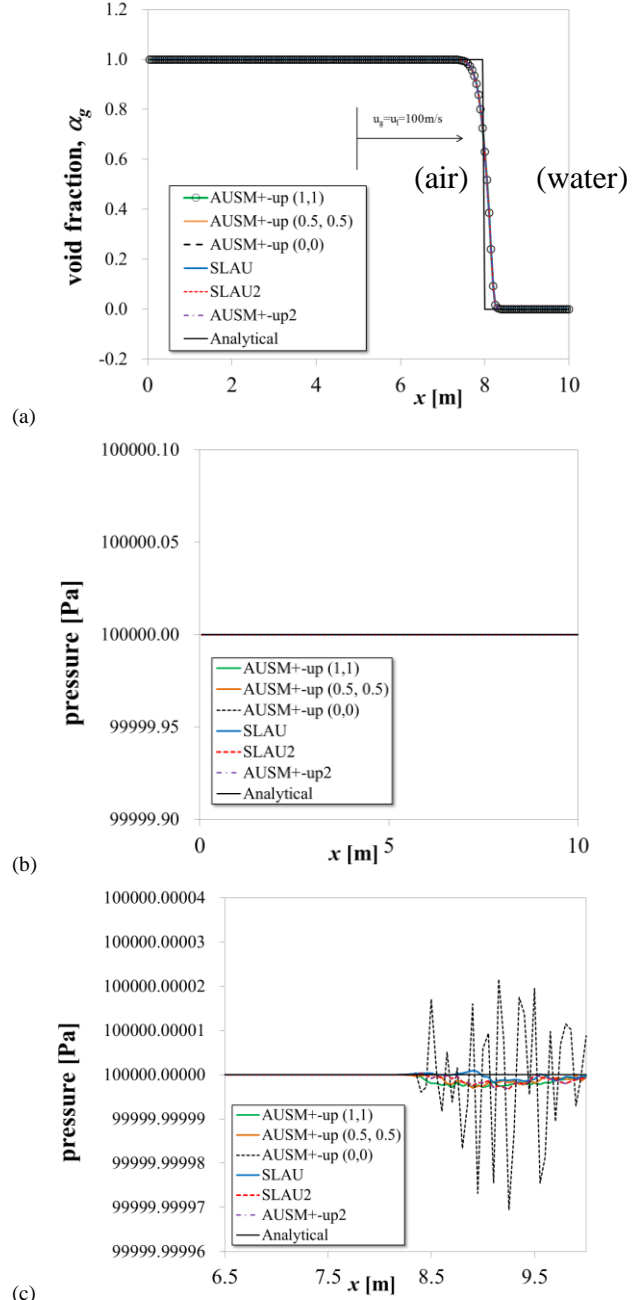


Figure 3: Moving Phase Contact Discontinuity Solutions at  $t=0.03s$  (a) Void fraction,  $\alpha_g$ ; (b) Pressure; (c) Pressure (expanded scale).

As the first problem, a moving contact discontinuity between air and water separated at  $x=5\text{m}$  [13] is solved. It is desired to accurately capture this phase discontinuity across which pressure constancy should be maintained. 200 uniform cells are used for  $[0\text{m}, 10\text{m}]$  domain (hence, the grid spacing  $\Delta x=0.05\text{m}$ ), and the initial conditions are given as:

- $(p, \alpha_g, u_k, T_k)_L = (10^5 \text{ Pa}, 1-\varepsilon, 100 \text{ m/s}, 0 \text{ m/s}, 300\text{K})$  for  $x \leq 5\text{m}$
- $(p, \alpha_g, u_k, T_k)_R = (10^5 \text{ Pa}, \varepsilon, 100 \text{ m/s}, 0 \text{ m/s}, 300\text{K})$  for  $x > 5\text{m}$

where  $k=g, l$ , and  $\varepsilon=1.0 \times 10^{-7}$  ( $\varepsilon_{\min}=1.0 \times 10^{-8}$ ,  $\varepsilon_{\max}=1.0 \times 10^{-4}$ ). The computations are conducted with  $\Delta t=6.0 \times 10^{-6}\text{s}$  ( $\text{CFL} \approx 0.2$ ), up to  $0.03\text{s}$  (5,000 steps).

The results are shown in Fig. 3. All the fluxes tested except for AUSM<sup>+</sup>-up (Niu) and AUSMPW+ showed excellent performance both in smooth transition of the two phases (Fig. 3a) and in preserving pressure across them (Fig. 3b). When the pressure is expanded as in Fig. 3c, however, there are from  $O(10^{-6})$  to  $O(10^{-5})$  [Pa] of disturbances downstream the interface with different profiles; but still, they are negligibly small, compared with the initial uniform pressure,  $10^5$  [Pa], and freestream liquid pressure,  $8.5 \times 10^8$  [Pa]. AUSM<sup>+</sup>-up (Niu) led to divergence of computation due to inappropriate dissipation, and AUSMPW+ also failed [if the weight function is not used, i.e., Eq. (12a) is employed rather than Eq. (17a), it worked. This form, however, almost corresponds to AUSM<sup>+</sup>-up (0, 0)].

### 3.2 Faucet Problem (Two-Phase Flow)

The second test is the well-known ‘Faucet’ problem dealing with a water jet injected with  $10\text{m/s}$  and accelerated by gravity downward (and hence, narrowed, according to the mass conservation law) surrounded by a stationary air, in a  $12\text{m}$  length tube  $[0\text{m}, 12\text{m}]$ . This problem is usually modeled by the following initial conditions:

- $(p, \alpha_g, u_g, u_l, T_g, T_l) = (10^5 \text{ Pa}, 0.2, 0 \text{ m/s}, 10 \text{ m/s}, 300\text{K}, 300\text{K})$

The same set is applied to the inlet boundary condition, except for pressure which is extrapolated from the interior cell; whereas pressure of  $10^5 \text{ Pa}$  is specified and other variables are extrapolated from interior cells at the outlet. Note that the gas and liquid velocities are set differently not as in [9, 13] but as in [12, 15, 16]. It is a feature of the two-fluid model that different velocities are allowed within a single cell, in contrast to one-fluid model having only one velocity according to velocity-equilibrium assumption [9]. Only in this test case,  $(g_x, g_x) = (9.8\text{m/s}^2, 0\text{m/s}^2)$  is activated in the source term of Eq. (1b) in order to reproduce the gravity effects accelerating the water downward ( $+x$ -

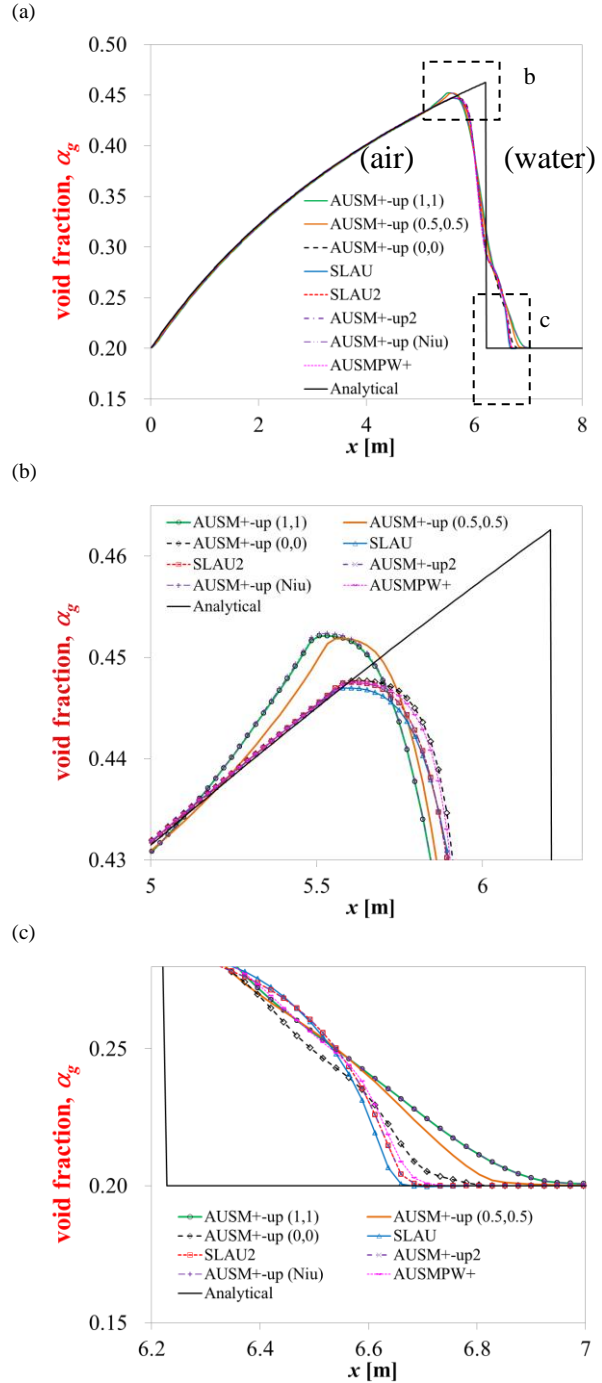


Figure 4: Faucet Problem Solutions at  $t=0.5\text{s}$  (a) Overview; (b) Blow-up view of top of wave front; (c) Blow-up view of bottom of wave front.

direction).

As a default grid, the following uniform cells and time step are used:

- 500 cells:  $\Delta x=0.024\text{m}$ ,  $\Delta t=1.0\times 10^{-5}\text{s}$  (CFL $\approx 0.63$ ), computations up to 0.5s (50,000 steps)  
[Default Grid]

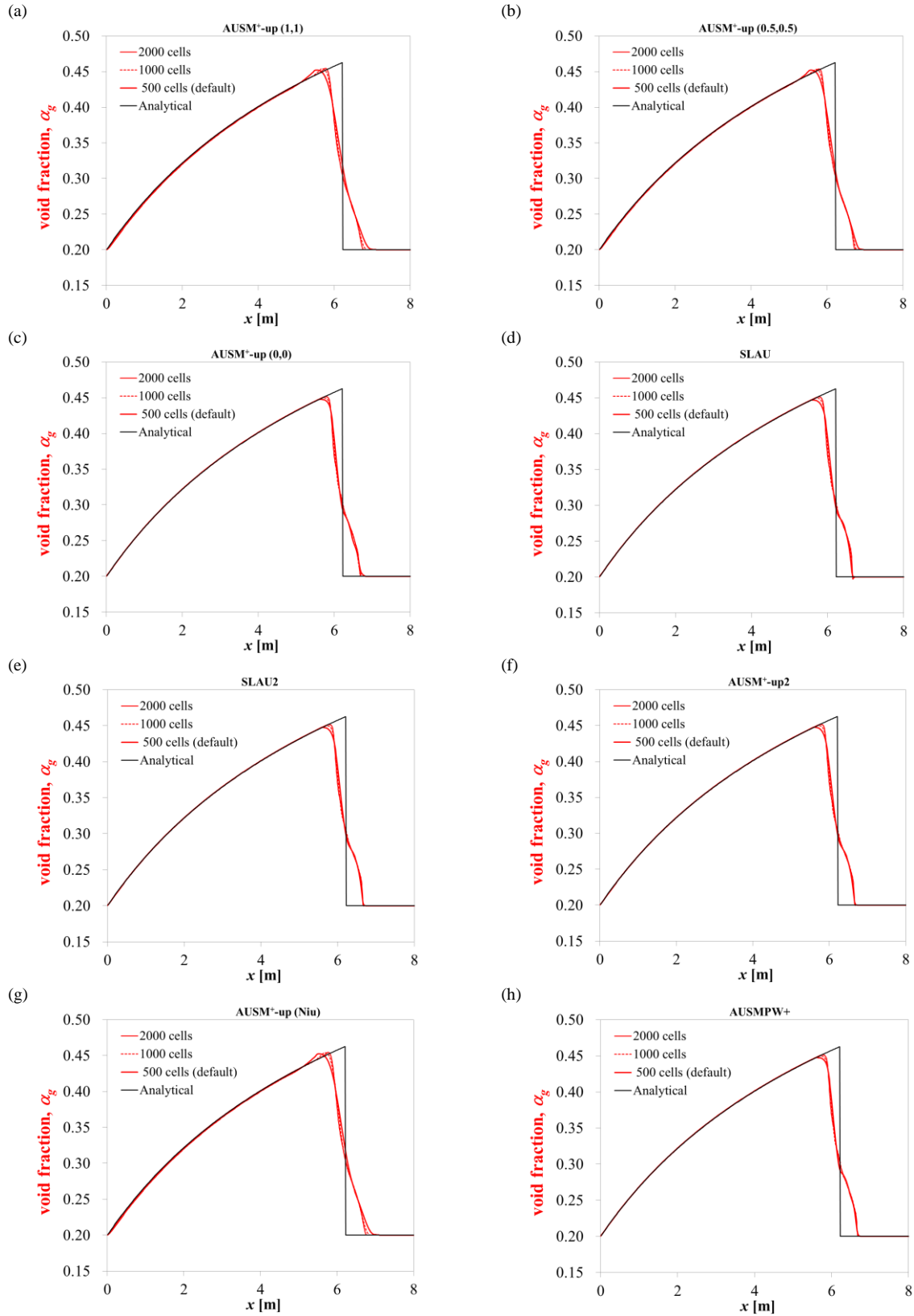


Figure 5: Faucet Problem Solutions at  $t=0.5\text{s}$  (a)  $\text{AUSM}^+\text{-up} (1, 1)$ ; (b)  $\text{AUSM}^+\text{-up} (0.5, 0.5)$ ; (c)  $\text{AUSM}^+\text{-up} (0, 0)$ ; (d) SLAU; (e) SLAU2; (f)  $\text{AUSM}^+\text{-up}2$ ; (g)  $\text{AUSM}^+\text{-up} (\text{Niu})$ ; (h) AUSMPW+.

whereas in the grid convergence study, the following denser grids are used with different time steps:

- 1,000 cells:  $\Delta x=0.012\text{m}$ ,  $\Delta t=5.0\times 10^{-6}$  (CFL $\approx 0.63$ ), computations up to 0.5s (100,000 steps) [Fine Grid]
- 2,000 cells:  $\Delta x=0.006\text{m}$ ,  $\Delta t=2.5\times 10^{-6}$  (CFL $\approx 0.63$ ), computations up to 0.5s (200,000 steps) [Very Fine Grid]

The computed results are compared with the following analytical solution [15]:

$$\alpha_g(x,t) = \begin{cases} 1 - \frac{(1 - \alpha_g(0,0)) \cdot u_l(0,0)}{\sqrt{(u_l(0,0))^2 + 2g_x x}} & \text{if } x < \frac{gt^2}{2} + u_l(0,0) \cdot t \\ \alpha_g(0,0) & \text{else} \end{cases} \quad (24)$$

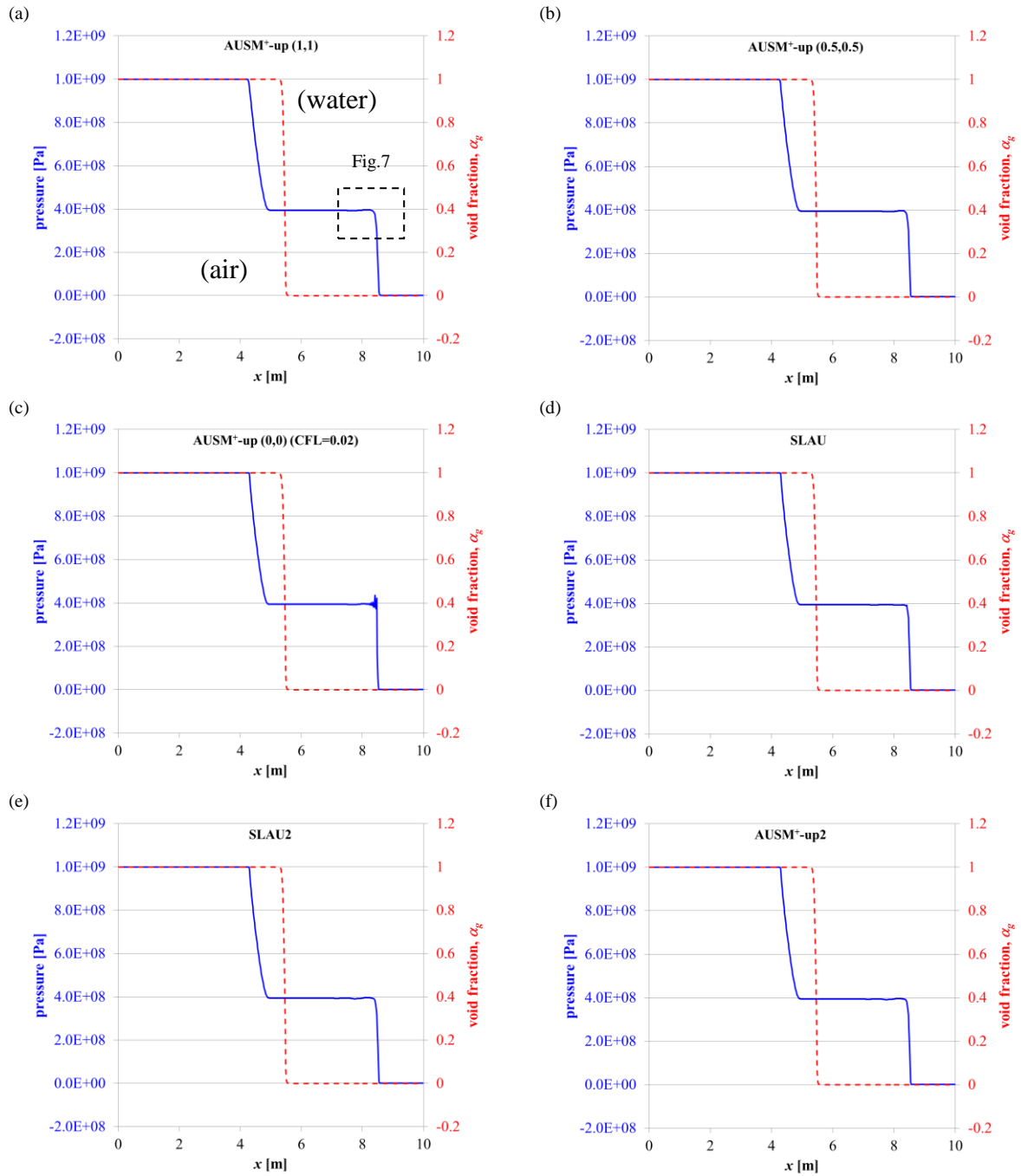


Figure 6: air-to-water shock tube problem solutions at  $t=2\text{ms}$ , (a) AUSM<sup>+</sup>-up (1, 1); (b) AUSM<sup>+</sup>-up (0.5, 0.5); (c) AUSM<sup>+</sup>-up (0, 0); (d) SLAU; (e) SLAU2; (f) AUSM<sup>+</sup>-up2

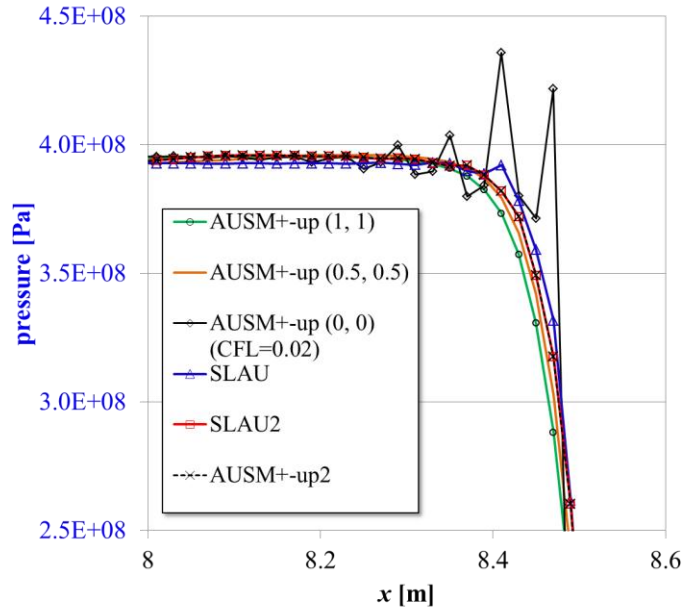


Figure 7: Magnified View of Pressure Profiles near Shock Front in Water, at  $t=2\text{ms}$  of the Air-to-Water Shock Tube Problem

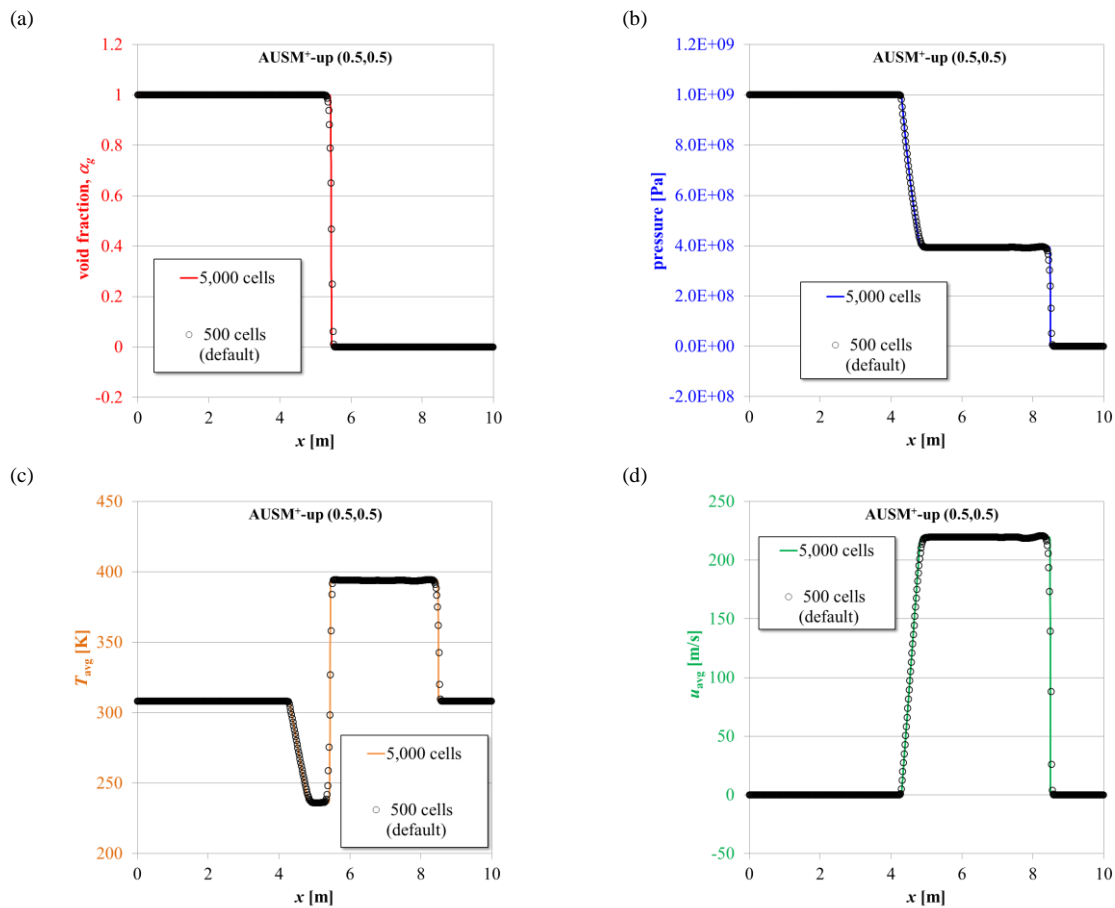


Figure 8: Solutions showing Grid Convergence at  $t=2\text{ms}$  of the Air-to-Water Shock Tube Problem of AUSM<sup>+</sup>-up (0.5, 0.5) (a) Void fraction; (b) Pressure; (c) Averaged temperature; (d) Averaged velocity.

The results of the default grid are shown in Fig. 4. AUSM<sup>+</sup>-up (1, 1) and (0.5, 0.5) showed slight overshoots at the top of the wave front (Fig. 4b), whereas the others exhibit slightly abrupt drop at the bottom (Fig. 4c); but in general, all the flux functions yielded almost the same, smooth profiles without serious oscillations (Fig. 4a).

As shown in Fig. 5, grid convergence is achieved with smooth profile for each flux function, even for AUSM<sup>+</sup>-up (0, 0) having no low speed cares. From the next example, however, steep pressure gradients will appear and affect the solution.

### 3.3 Shock tube problems

As a preliminary investigation, we had solved an underwater shock tube problem, showing behaviors of each flux function at a very low Mach number in water: AUSM<sup>+</sup>-up (1, 1) and AUSM<sup>+</sup>-up (Niu) captured a shock and a rarefaction wave in the most smooth but slightly diffused manner; AUSM<sup>+</sup>-up (0.5, 0.5) looked a good balance; SLAU, SLAU2, and AUSM<sup>+</sup>-up2 exhibit slight oscillations yet reduced with a special care; AUSM<sup>+</sup>-up (0, 0) showed catastrophic profile; AUSMPW+ was not able to compute this problem (see Appendix B for details). Keeping them in mind, we will deal with shock tube problems involving a propagating shock from air to water, or vice versa.

#### 3.3.1 Air-to-Water Shock Tube (Two-Fluid Flow)

As in the moving contact discontinuity problem, a 1D domain of [0m, 10m] is separated by left and right states at  $x=5m$ , but with the following different conditions:

- $(p, \alpha_g, u_k, T_k)_L = (10^9 \text{ Pa}, 1-\varepsilon, 100 \text{ m/s}, 0 \text{ m/s}, 308.15\text{K})$  for  $x \leq 5m$
- $(p, \alpha_g, u_k, T_k)_R = (10^5 \text{ Pa}, \varepsilon, 100 \text{ m/s}, 0 \text{ m/s}, 308.15\text{K})$  for  $x > 5m$

where  $k=g, l$ , and  $\varepsilon=1.0 \times 10^{-7}$  ( $\varepsilon_{\min}=1.0 \times 10^{-8}$ ,  $\varepsilon_{\max}=1.0 \times 10^{-4}$ ), again. A default grid composed of the following uniform cells with time step is used:

- 500 cells:  $\Delta x=0.02m$ ,  $\Delta t=2.0 \times 10^{-6}s$  (CFL $\approx 0.2$ ), computed up to  $2.0 \times 10^{-3}s$  (1,000 steps) [*Default Grid*]

The following additional grid with a different time step is used for grid convergence study:

- 5,000 cells:  $\Delta x=0.002m$ ,  $\Delta t=2.0 \times 10^{-7}s$  (CFL $\approx 0.2$ ), computed up to  $2.0 \times 10^{-3}s$  (10,000 steps) [*Fine Grid*]

The results for all the fluxes are shown in Fig. 6. AUSM<sup>+</sup>-up (0, 0) required a smaller time step ( $\Delta t=2.0 \times 10^{-7}s$ ; CFL $\approx 0.02$ ), because otherwise the computation diverged. Even with this time step, AUSM<sup>+</sup>-up (Niu) and AUSMPW+ drove divergence soon at the phase interface, thus, the results are not shown. All the cases displayed smoothly captured a rarefaction wave in air ( $x \approx 4.5m$ ), a phase interface between air and water ( $x \approx 5.5m$ ), and a shock in water ( $x \approx 8.5m$ ), except for AUSM<sup>+</sup>-up (0, 0) showing slight oscillations at shock front (Fig. 6c). This is clearly seen in the magnified view of the top of the shock front in Fig. 7, in which all the computed cases are compared. AUSM<sup>+</sup>-up (1, 1), AUSM<sup>+</sup>-up (0.5, 0.5), SLAU2, AUSM<sup>+</sup>-up2 are smooth, and the last two, sharing the common pressure flux, are indistinguishable. SLAU showed a slight kink due to smaller dissipation, but not severely. AUSM<sup>+</sup>-up (0, 0), having insufficient dissipation, showed large variation of pressure at the shock (although the local velocity there was approximately 220 [m/s], not very slow). Furthermore, grid convergence is achieved for each flux except for AUSM<sup>+</sup>-up (0, 0), AUSM<sup>+</sup>-up (Niu), and AUSMPW+, when compared with the case using 5,000 cells, as shown in Fig. 8 represented by AUSM<sup>+</sup>-up (0.5, 0.5).

#### 3.3.2 Water-to-Air Shock Tube (Two-Fluid Flow)

Now the same grid system is used as in the air-to-water shock tube with the following setup:

- $(p, \alpha_g, u_k, T_k)_L = (1 \times 10^7 \text{ Pa}, \varepsilon, 100 \text{ m/s}, 0 \text{ m/s}, 308.15\text{K})$  for  $x \leq 5m$
- $(p, \alpha_g, u_k, T_k)_R = (5 \times 10^6 \text{ Pa}, 1-\varepsilon, 100 \text{ m/s}, 0 \text{ m/s}, 308.15\text{K})$  for  $x > 5m$

with the following default grid and time step:

- 500 cells:  $\Delta x=0.02m$ ,  $\Delta t=2.0 \times 10^{-6}s$  (CFL $\approx 0.2$ ), up to  $2.0 \times 10^{-3}s$  (1,000 steps) [*Default Grid*]

whereas the fine grid for grid convergence study used:

- 5,000 cells:  $\Delta x=0.002m$ ,  $\Delta t=2.0 \times 10^{-7}s$  (CFL $\approx 0.2$ ), up to  $2.0 \times 10^{-3}s$  (10,000 steps) [*Fine Grid*]

The results for AUSM<sup>+</sup>-up (1, 1), (0.5, 0.5), and (0, 0), SLAU, SLAU2, and AUSM<sup>+</sup>-up2 are shown

in Fig. 9. Again, AUSM<sup>+</sup>-up (Niu) and AUSMPW+ were not able to compute this problem, thus, the results are not shown. In this test, AUSM<sup>+</sup>-up (0, 0) exhibited severe pressure oscillations in the water portion of the middle region where Mach number is of the order of  $O(10^{-3})$  (Fig. 9c) as in the underwater shock tube in Appendix B. The other methods seemed free from such oscillations, showing reasonable capturing of a rarefaction wave in water (which is very steep compared with the one in air) ( $x \approx 2$ m), smooth transition at a phase interface ( $x \approx 5$ m), and robust capturing of a shock in air (which looks very weak) ( $x \approx 6$ m). In Fig. 10 the foot of the strong rarefaction is closed up for comparison of different flux functions. As in the previous problem, AUSM<sup>+</sup>-up (1, 1) is the most smooth, followed by AUSM<sup>+</sup>-up (0.5, 0.5). AUSM<sup>+</sup>-up (0, 0) is totally erratic, and the other methods show slight undershoots. Grid convergence is, again, confirmed for AUSM<sup>+</sup>-up (0.5, 0.5) in Fig. 11.

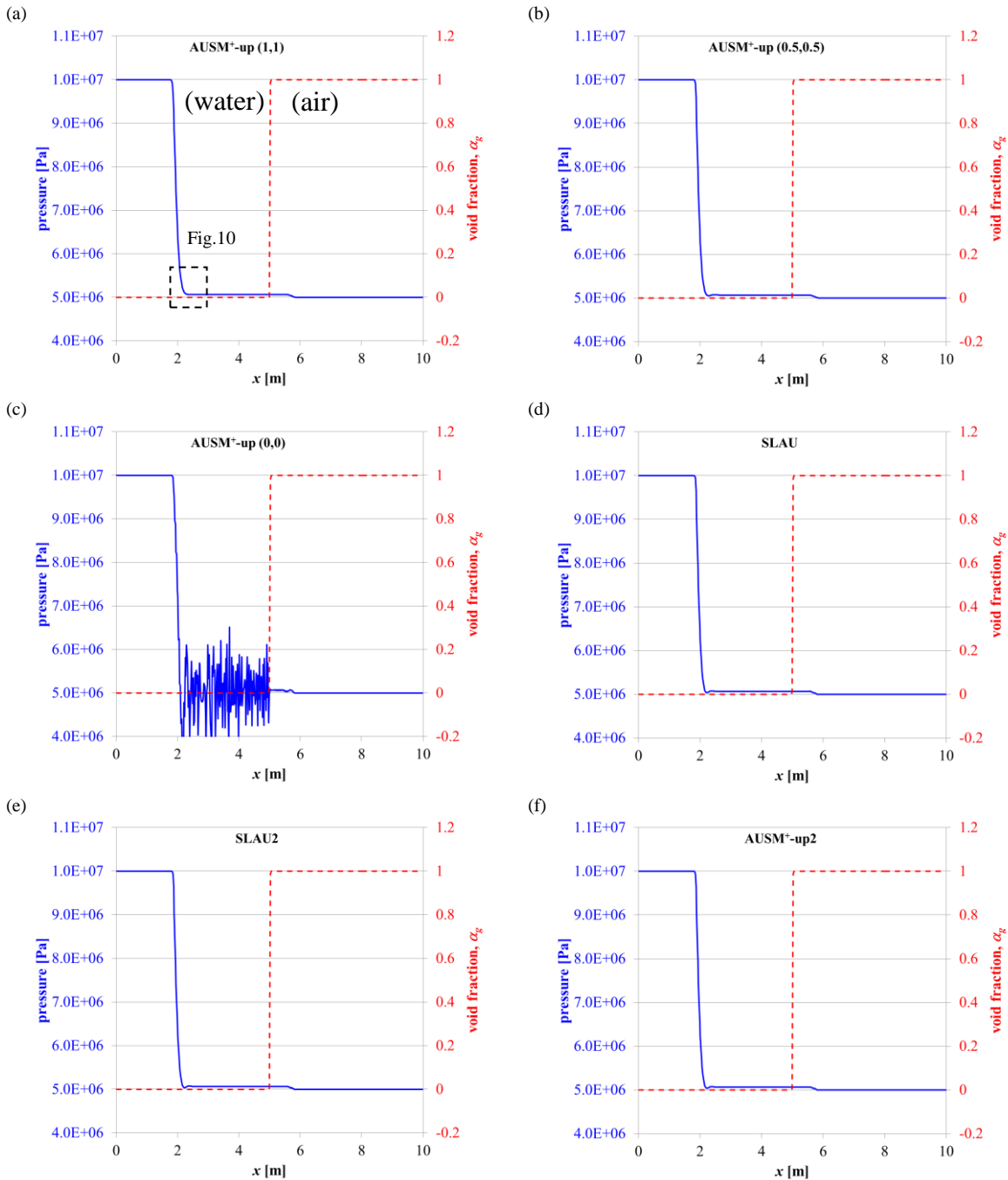


Figure 9: Water-to-Air Shock Tube Problem Solutions at  $t=2$ ms, (a) AUSM<sup>+</sup>-up (1, 1); (b) AUSM<sup>+</sup>-up (0.5, 0.5); (c) AUSM<sup>+</sup>-up (0, 0); (d) SLAU; (e) SLAU2; (f) AUSM<sup>+</sup>-up2

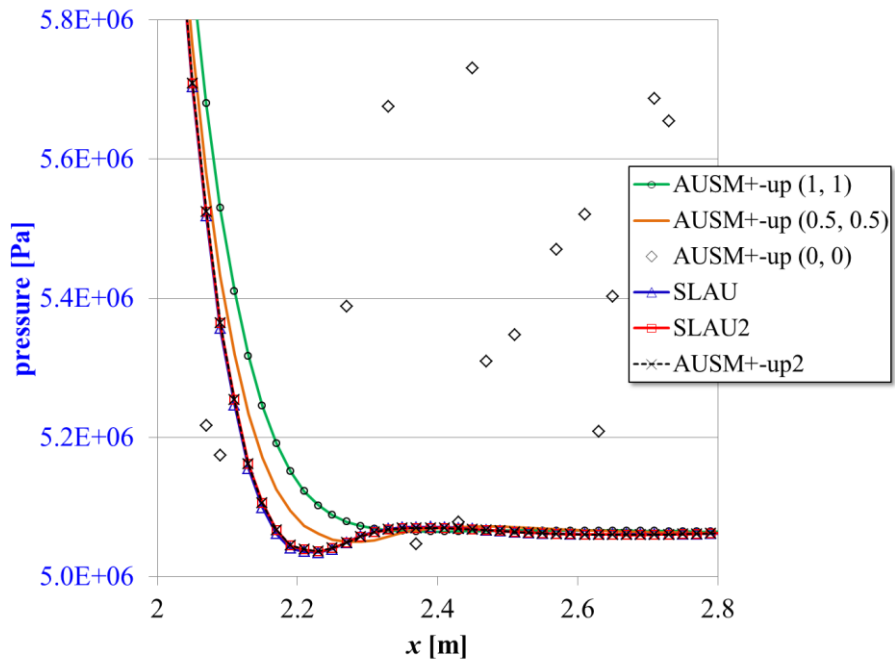


Figure 10: Magnified View of Pressure Profiles around Foot of Expansion Wave in Water, at  $t=2\text{ms}$  of the Water-to-Air Shock Tube Problem

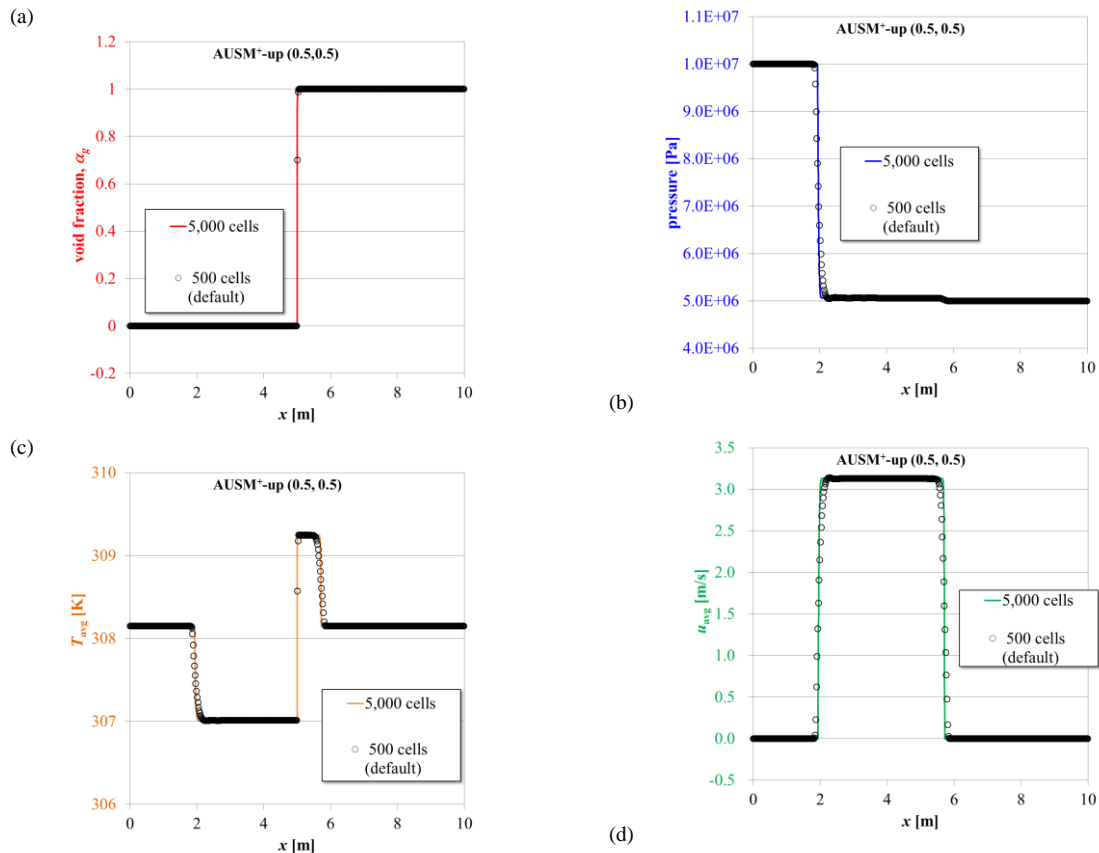


Figure 11: Solutions showing Grid Convergence at  $t=2\text{ms}$  of the Water-to-Air Shock Tube Problem of AUSM<sup>+</sup>-up (0.5, 0.5), (a) Void fraction; (b) Pressure; (c) Averaged temperature; (d) Averaged velocity.

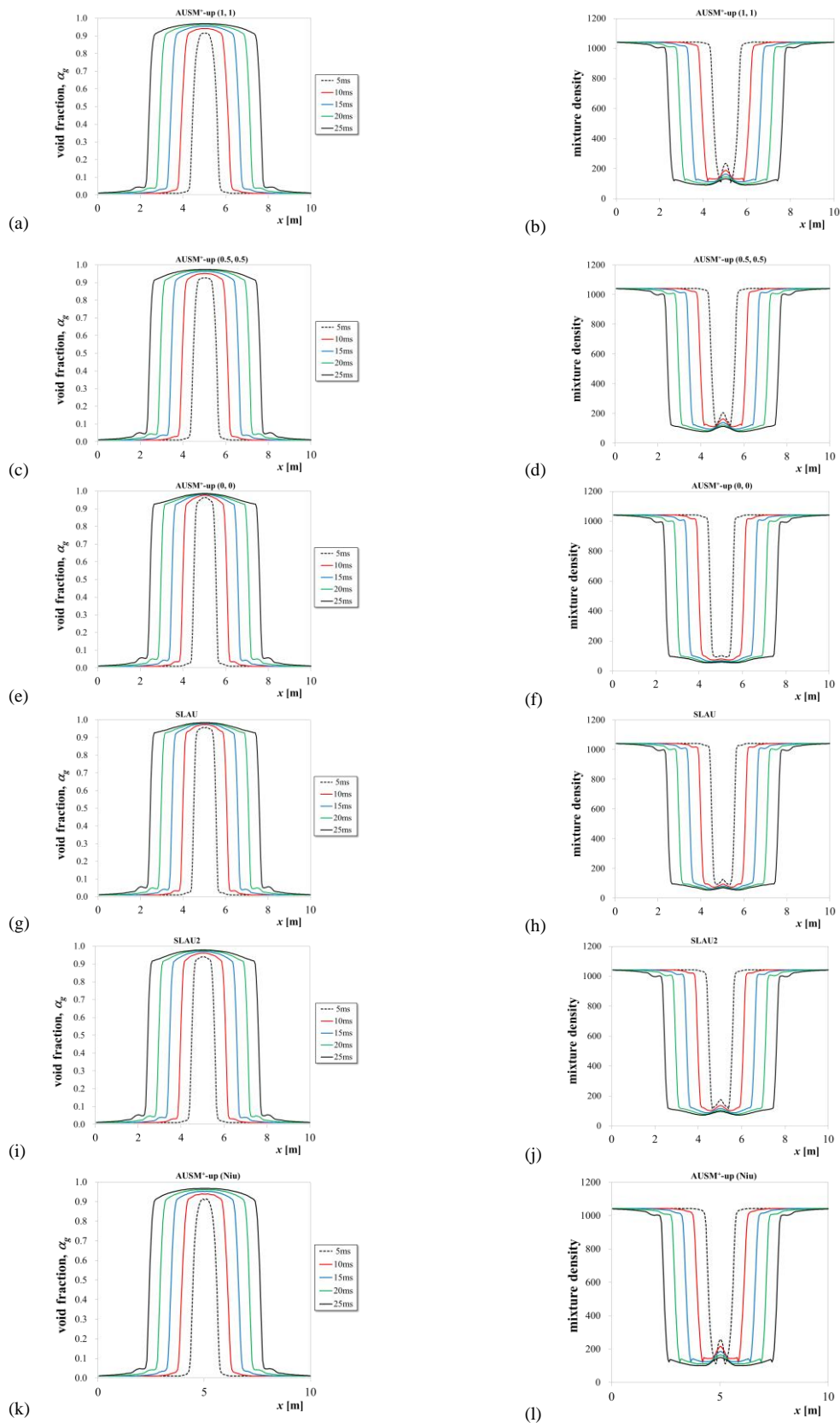


Figure 12: 1D Cavitation Problem Results at  $t=25\text{ms}$  (a)  $\text{AUSM}^+\text{-up (1,1)}$ , void fraction,  $\alpha_g$ ; (b)  $\text{AUSM}^+\text{-up (1,1)}$ , averaged density; (c)  $\text{AUSM}^+\text{-up (0.5,0.5)}$ ,  $\alpha_g$ ; (d)  $\text{AUSM}^+\text{-up (0.5,0.5)}$ , averaged density; (e)  $\text{AUSM}^+\text{-up (0,0)}$ ,  $\alpha_g$ ; (f)  $\text{AUSM}^+\text{-up (0,0)}$ , averaged density; (g) SLAU,  $\alpha_g$ ; (h) SLAU, averaged density; (i) SLAU2,  $\alpha_g$ ; (j) SLAU2, averaged density; (k)  $\text{AUSM}^+\text{-up (Niu)}$ ,  $\alpha_g$ ; (l)  $\text{AUSM}^+\text{-up (Niu)}$ , averaged density.

### 3.4 1D Cavitation Problem (Two-Phase Flow)

This test was proposed by Saurel and Abgrall in [16], in which receding liquid flow containing 1% gas in a tube dynamically creates a cavitation zone at the center. As the problem setup, 200 cells are uniformly distributed over the [0m, 10m] domain (i.e., the grid spacing is  $\Delta x=0.05\text{m}$ ), and the initial conditions are given as:

- $(p, \alpha_g, u_k, T_k)_L = (10^5 \text{ Pa}, \varepsilon, -100 \text{ m/s}, 300\text{K})$  for  $x \leq 5\text{m}$
- $(p, \alpha_g, u_k, T_k)_R = (10^5 \text{ Pa}, \varepsilon, 100 \text{ m/s}, 300\text{K})$  for  $x > 5\text{m}$

where  $k=g, l$ , and  $\varepsilon=1.0 \times 10^{-2}$  ( $\varepsilon_{\min}=1.0 \times 10^{-3}$ ,  $\varepsilon_{\max}=1.0 \times 10^{-1}$ ). The computations are conducted with  $\Delta t=5.0 \times 10^{-6}\text{s}$  ( $\text{CFL} \approx 0.16$ ), up to 25ms (5,000 steps).

Fig. 12 shows the results. AUSM<sup>+</sup>-up2, which showed identical results to SLAU2, and AUSMPW+, which failed to compute this problem, are omitted. It has been demonstrated that, as in Saurel and Abgrall's more elaborate, relaxation-involved method, "even starting from a situation in which interfaces are not present," most of fluxes, including AUSM<sup>+</sup>-up (Niu) this time, are "capable of dynamically creating interfaces," as stated in [16]. This feature motivates us to go on to more realistic cavitation problems in future.

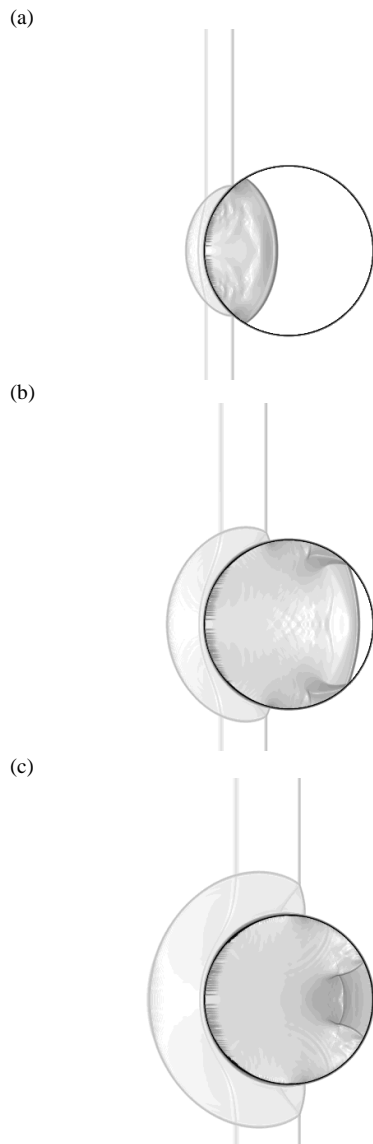


Figure 13: time evolution of solution of shock/water-droplet interaction problem of AUSM<sup>+</sup>-up (1, 1) (a)  $t = 3.75 \mu\text{s}$ ; (b)  $t = 5.25 \mu\text{s}$ ; (c)  $t = 6.75 \mu\text{s}$  (numerical Schlieren).

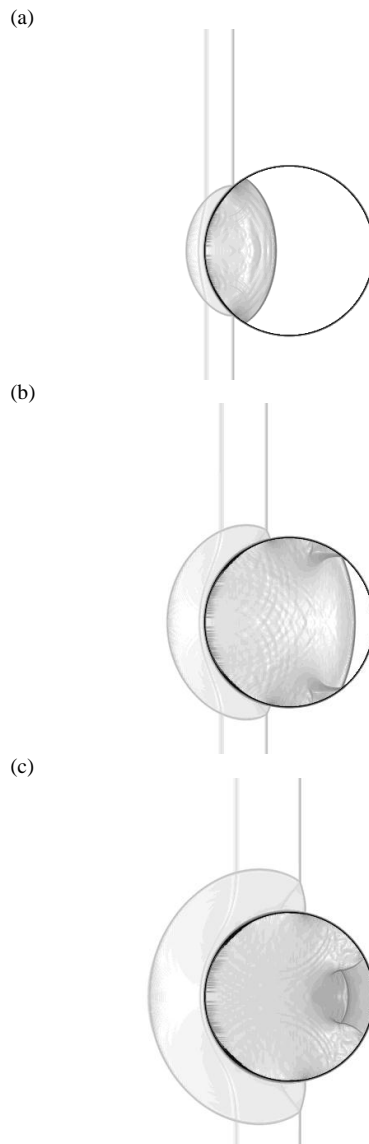


Figure 14: time evolution of solution of shock/water-droplet interaction problem of AUSM<sup>+</sup>-up (0.5, 0.5) (a)  $t = 3.75 \mu\text{s}$ ; (b)  $t = 5.25 \mu\text{s}$ ; (c)  $t = 6.75 \mu\text{s}$  (numerical Schlieren).

### 3.5 Shock/Water-Column Interaction (Two-Fluid Flow, 2D)

As the final and realistic example, a shock in air impacting on a water-column (i.e., 2D droplet) is simulated.  $400 \times 200$  isotropic cells are used for a domain of  $[-5\text{mm}, 5\text{mm}] \times [0\text{mm}, 5\text{mm}]$  to cover the  $6.4\text{mm}$  diameter water column with its center at origin, i.e., the diameter being 256 times grid spacing  $\Delta x_{\min} = \Delta y_{\min} = 0.025\text{mm}$  in this region; then the cells are stretched toward outer boundaries so that a domain of  $[-15\text{mm}, 20\text{mm}] \times [0\text{mm}, 15\text{mm}]$  is filled with  $900 \times 420$  cells as a total.

The initial conditions are as the same as in [14]:

- $(p, \alpha_g, u_k, v_k, T_k)_L = (2.35438 \times 10^5 \text{ Pa}, \varepsilon, 225.86 \text{ m/s}, 0 \text{ m/s}, 381.85\text{K})$  for  $x \leq -4\text{mm}$
- $(p, \alpha_g, u_k, v_k, T_k)_R = (1 \times 10^5 \text{ Pa}, \varepsilon, 0 \text{ m/s}, 0 \text{ m/s}, 293.15\text{K})$  for  $x > 4\text{mm}$ , except for  $x^2 + y^2 < (3.2\text{mm})^2$  where  $\alpha_g = 1 - \varepsilon$

where  $k=g, l$ , and  $\varepsilon = 1.0 \times 10^{-5}$  ( $\varepsilon_{\min} = 1.0 \times 10^{-5}$ ,  $\varepsilon_{\max} = 1.0 \times 10^{-4}$ ). Then the shock starts to move with  $M_{sh} = 1.47$  at  $t=0$ , and hits the water-column at  $t \approx 1.5\mu\text{s}$ . The computations are carried out with  $\Delta t = 1.25 \times 10^{-9}\text{s}$  ( $\text{CFL} \approx 0.3$ ) up to  $10\mu\text{s}$  (8,000 steps).

Since the air/water interface having a circular shape should reside on the Cartesian-type grid, we specified a smooth transition region of  $\pm 2\Delta x_{\min}$  width on the initial phase interface so that the void fraction  $\alpha_g$  is interpolated using the same blending function applied for “vanishing” phase treatment:

$$(\alpha_g)_{adjust} = G(\xi_2) \cdot \varepsilon + (1 - G(\xi_2)) \cdot (1 - \varepsilon) \quad (25a)$$

$$G(\xi_2) = -\xi_2^2 (2\xi_2 - 3) \quad (25b)$$

$$\xi_2 = \frac{\sqrt{x^2 + y^2} - (r - 2\Delta x_{\min})}{4\Delta x_{\min}}, \quad r - 2\Delta x_{\min} \leq \sqrt{x^2 + y^2} \leq r + 2\Delta x_{\min}, \quad r = 3.2\text{mm} \quad (25c)$$

At the bottom boundary, the conventional slip condition is imposed, i.e., only the  $y$ -component velocity is reflected, while the other variables are simply extrapolated from the interior cells. The other boundaries are typical: the left boundary is the inlet condition, the right is the outlet, and the top boundary is the side. Those far field boundaries are far away from the water-column enough to prevent the influence to the problem.

The results are shown in Figs. 13-15 (in which numerical Schlieren function  $(1 + \alpha_i^2) \log(|\nabla \rho| + 1)$  [13] is used with the range between 4 and 28) for AUSM<sup>+</sup>-up (1, 1), AUSM<sup>+</sup>-up (0.5, 0.5), and SLAU2. AUSM<sup>+</sup>-up2 results are very similar to those of SLAU2, thus, omitted. AUSM<sup>+</sup>-up (0, 0), SLAU, AUSM<sup>+</sup>-up (Niu), and AUSMPW+ were unable to compute this problem.

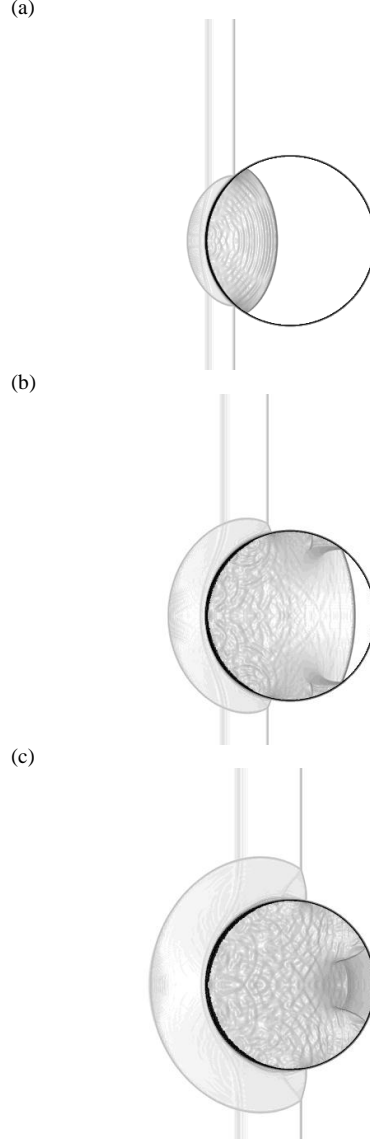


Figure 15: time evolution of solution of shock/water-droplet interaction problem of SLAU2 (a)  $t = 3.75\mu\text{s}$ ; (b)  $t = 5.25\mu\text{s}$ ; (c)  $t = 6.75\mu\text{s}$  (numerical Schlieren).

AUSM<sup>+</sup>-up (1, 1) in Fig. 13 shows similar results evolved with time as in [14]. After impacting on the water-column, the shock transmits into the water region; in the air region, on the other hand, it diffracts as if it began to glance around a solid object ( $t = 5\mu\text{s}$ , Figs. 13a). Then, as seen in Figs 13b, the shock travels faster inside the water-column than outside because of the greater speed of sound. At  $t = 6.75\mu\text{s}$ , the shock in the water-column has reflected from the rear phase interface (Figs. 13c).

AUSM<sup>+</sup>-up (0.5, 0.5), less diffusive than AUSM<sup>+</sup>-up (1, 1), shows very similar solutions overall (Fig. 14) but with a slightly non-smooth inside-water profile in Fig. 14c. Thus, although AUSM<sup>+</sup>-up (0.5, 0.5) looked a good balance for some of the previous test cases, AUSM<sup>+</sup>-up (1, 1) may be better for challenging problems like this test. SLAU2 in Fig. 15, again, still resolves flow features yet with slightly more oscillations in the water-column. Thus, SLAU2 (and AUSM<sup>+</sup>-up2) may be used, when those (weak) oscillations are acceptable, or in combination with the exact Riemann solver, as briefly introduced in Appendix C (which will be further studied as a future work).

All in all, AUSM<sup>+</sup>-up (1, 1), AUSM<sup>+</sup>-up (0.5, 0.5), and SLAU2 solutions are roughly similar, yet with different smoothness/diffusiveness in this order, as in all the other tests. Still, more importantly, those methods have been successfully extended for multifluid and multiphase flows including such a two-dimensional, challenging problem. The results of all the test problems with all the flux functions are summarized in Tables 1.

Table 1. List of solutions of test problems (S: Successful, A: Acceptable, F: Failure)

Flux functions (listed in order of smoothness/diffusiveness of solutions in general)	3.1 Moving phase discontinuity (Two-fluid)	3.2 Faucet problem (Two-phase)	3.3.1 Air-to-water shock tube (Two-fluid)	3.3.2 Water-to-air shock tube (Two-fluid)	3.4 1D cavitation (Two-phase)	3.5 Shock/water-column interaction (Two-fluid, 2D)
AUSM <sup>+</sup> -up (1, 1)	S	S	S	S	S	S
AUSM <sup>+</sup> -up (0.5, 0.5)	S	S	S	S	S	A (slightly oscillatory)
SLAU2 or AUSM <sup>+</sup> -up2	S	S	S	A (slight undershoot)	S	A (weakly oscillatory)
SLAU	S	S	A (slight oscillation)	A (slight undershoot)	S	F (diverge)
AUSM <sup>+</sup> -up (0, 0)	S	S	F (oscillatory)	F (oscillatory)	S	F (diverge)
AUSM <sup>+</sup> -up (Niu)	F (diverge)	S	F (diverge)	F (diverge)	S	F (diverge)
AUSMPW+	F (diverge)	S	F (diverge)	F (diverge)	F (diverge)	F (diverge)

## 4 Conclusions

Following Liou et al. [14], recently-developed, AUSM-family numerical flux functions have been successfully extended to compressible multifluid and multiphase flow computations, based on the stratified flow model concept. Then, we carried out an extensive survey using those flux functions. The key findings are as follows:

- AUSM<sup>+</sup>-up with large dissipation parameters for low speeds ( $K_p=K_u=1$ ), that with small dissipation ( $K_p=K_u=0.5$ ), and SLAU2 or AUSM<sup>+</sup>-up2 ( $K_p=1$ ) can be used in all the problems solved here (with this order of smoothness/diffusivity of solutions), even in a challenging 2D shock/water-droplet interaction.
- SLAU showed oscillatory behaviors [though not as catastrophic as those of AUSM<sup>+</sup>, i.e., AUSM<sup>+</sup>-up ( $K_p=K_u=0$ )] due to insufficient dissipation arising from inherent limitation in extension of its dissipation term.
- AUSM<sup>+</sup>-up modified by Niu et al. [17] and AUSMPW+ are applicable to limited, two-phase flow test cases having no steep pressure gradients. The former has problem-dependent dissipation which is inappropriate to the other problems, and the latter has weight functions that behaved adversely under the water.

We hope the results and discoveries here will serve as a guideline for users when choosing fluxes in particular problems, and also they will help us with further developments of numerical modeling of

multiphase flows.

## Acknowledgements

This work is supported by Grant-in-Aid for Young Research Fellows of Japan Society for the Promotion of Science (JSPS), Japan. Computational resources are provided by Center for Risk Studies and Safety, University of California, Santa Barbara, and Ohio Aerospace Institute, Cleveland. We thank all those contributors. We are grateful to Dr. Chih-Hao Chang at University of California, Santa Barbara, USA, for providing us with helpful advices continuously as well as his sample codes. We also thank Dr. Hiroshi Terashima at University of Tokyo, Japan, Dr. Taku Nonomura at JAXA, Japan, Dr. Ashvin Hosangadi of Combustion Research and Flow Technology (CRAFT Tech), Inc., USA, Dr. Eiji Shima at JEDI center, JAXA, Japan, and Professor Yang-Yao Niu at Chung Hua University, Taiwan, for their valuable comments.

## References

- [1] S. J. Osher and J. A. Sethian. *J. Comput. Phys.*, 79:12-49, 1988.
- [2] M. Sussman, P. Smereka, and S. Osher. *J. Comput. Phys.*, 114:146-159, 1994.
- [3] H. Kim and M.-S. Liou. *Comput. Fluids*, 44:111-129, 2011.
- [4] G. Tryggvason, B. Bunner, A. Esmaeeli, D. Juric, N. Al-Rawahi, W. Tauber, J. Han, S. Nas, and Y.-J. Jan. *J. Comput. Phys.*, 169:708–759, 2001.
- [5] H. Terashima and G. Tryggvason. *J. Comput. Phys.*, 228:4012-4037, 2009.
- [6] C. W. Hirt and B. D. Nichols. *J. Comput. Phys.*, 39:201–225, 1981.
- [7] S. Ii, K. Sugiyama, S. Takeuchi, S. Takagi, Y. Matsumoto, F. Xiao, *J. Comput. Phys.*, 231:2328–2358, 2012.
- [8] E. Goncalves and R. F. Patella. *Comput. Fluids*, 38:1682-1696, 2009.
- [9] J. R. Edwards, R. K. Franklin, and M.-S. Liou. *AIAA J.* 38:1624-1633, 2000.
- [10] S.-W. Ihm, and C. Kim. *AIAA J.*, 46:3012-3037, 2008.
- [11] R. Saurel and O. Lemetayer. *J. Fluid Mech.* 431:239-271, 2001.
- [12] I. Toumi. *Nuclear Sci. Eng.*, 123:147-168, 1996.
- [13] C.-H. Chang and M.-S. Liou. *J. Comput. Phys.*, 225:840-873, 2007.
- [14] M.-S. Liou, C.-H. Chang, L. Nguyen, and T. G. Theofanous. *AIAA J.*, 46:2345-2356, 2008.
- [15] H. Paillère, C. Corre, and J. R. G. Cascales. *Comput. Fluids*, 32:891–916, 2003.
- [16] R. Saurel and R. Abgrall, *J. Comput. Phys.*, 150:425–467, 1999.
- [17] Y.-Y. Niu, Y.-C. Lin, and C.-H. Chang. *Int. J. Numer. Meth. Fluids*, 58:879-896, 2008.
- [18] C.-H. Chang and M.-S. Liou, *AIAA Paper 2003-4107*, 2003.
- [19] C.-H. Chang, S. Sushchikh, L. Nguyen, M.-S. Liou, and T. Theofanous, *FEDSM2007-37338*, 2007.
- [20] R. K. Shukla, C. Pantano, and J. B. Freund. *J. Comput. Phys.*, 229:7411–7439, 2010.
- [21] C. C. Kiris, D. Kwak, W. Chan, J. A. Housman. *Comput. Fluids*, 37:536–546, 2008.
- [22] H. B. Stewart and B. Wendroff. *J. Comput. Phys.*, 56:363–409, 1984.
- [23] M.-S. Liou, *J. Comput. Phys.*, 214:137-170, 2006.
- [24] M.-S. Liou, *J. Comput. Phys.*, 129:364-382, 1996.
- [25] E. Shima and K. Kitamura. *AIAA J.*, 49:1693-1709, 2011.
- [26] K. Kitamura and E. Shima, *V European Conference on Computational Fluid Dynamics, ECCOMAS CFD 2010*, 2010.
- [27] K. Kitamura and E. Shima, *AIAA Paper 2011-3056*, 2011.
- [28] B. Van Leer. *J. Comput. Phys.*, 32:101-136, 1979.
- [29] G. D. Van Albada, B. Van Leer, and W. W. Roberts Jr. *Astron. Astrophys*, 108:76-84, 1982.
- [30] S. Gottlieb and C.-W. Shu. *Math. Comput.*, 67:73-85, 1998.
- [31] K. Kitamura, P. Roe, and F. Ismail. *AIAA J.*, 47:44-53, 2009.
- [32] J. Stuhmiller. *Int. J. Multiphase Flow*, 3:551–60, 1977.
- [33] F. Harlow and A. Amsden. *Fluid dynamics*, Technical Report LA-4700, Los Alamos National

Laboratory, 1971.

[34] K.H. Kim, C. Kim, and O.-H. Rho. J. Comput. Phys., 174:38–80, 2001.

[35] K. Kitamura, E. Shima, K. Fujimoto, and Z. J. Wang. Commun. Comput. Phys., 10:90-119, 2011.

[36] A. Hosangadi, J. Sachdev, and V. Sankaran, ICCFD7-2202, 2012.

## Appendix A: Limiter Effects

### A.1 Moving Phase Discontinuity with Different Flux Limiters (Two-Fluid Flow)

We had also surveyed effects of choosing flux limiter functions. The moving phase discontinuity results of AUSM<sup>+</sup>-up (1, 1) with the following limiters are compared: Van Albada [denoted as “VA,” with the limiter coefficient  $10^{-20}$  (default) or  $10^{-6}$ ], minmod, or Chakravarthy-Osher (denoted as “C-O,” which was adopted in Chang and Liou [13]), along with the MUSCL coefficient  $\kappa = -1$  (default; fully upwind 2nd-order) or  $1/3$  (upwind-biased 3rd-order). The results are shown in Fig. A1 in which pressure disturbance is closed up to the  $10^{-6}$  [Pa] level. It is seen that the C-O limiter (with either  $\kappa = -1$  or  $1/3$ ) has the best performance in preserving pressure constancy, but more importantly, any choice can suppress the pressure error within  $10^{-5}$  [Pa], which is 10 orders smaller than the uniform pressure.

Among these choices, we selected the Van Albada’s limiter with  $\kappa = -1$  as a default combination, because we found it the most robust combination in the challenging, shock/water-column test from our experience.

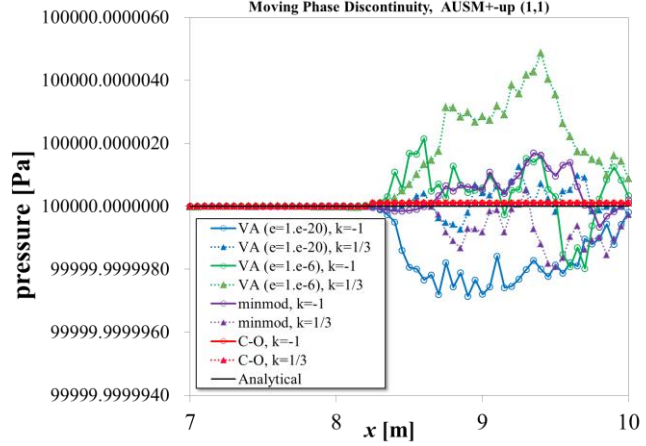


Figure A1: Magnified View of Limiter Effects on Pressure Disturbance from Moving Phase Contact Discontinuity

## Appendix B: Single-Liquid Flow

### B.1 Underwater Shock Tube (Single-Phase Flow)

As a preliminary study, we had solved an underwater shock tube problem and compared behaviors of flux functions at a very low Mach number in water. Following [14], a 1D domain of [0m, 1m] is prepared, the diaphragm was placed in the middle, and the initial conditions for the both sides were specified as below [18]:

- $(p, \alpha_g, u_k, T_k)_L = (10^6 \text{ Pa}, \varepsilon, 0 \text{ m/s}, 300\text{K})$  for  $x \leq 0.5\text{m}$
  - $(p, \alpha_g, u_k, T_k)_R = (10^5 \text{ Pa}, \varepsilon, 0 \text{ m/s}, 300\text{K})$  for  $x > 0.5\text{m}$
- where  $k=g, l$ , and  $\varepsilon = 1.0 \times 10^{-16}$  ( $\varepsilon_{\min} = 1.0 \times 10^{-16}$ ,  $\varepsilon_{\max} = 1.0 \times 10^{-12}$ ). The grid and time step are
- 200 cells:  $\Delta x = 0.005\text{m}$ ,  $\Delta t = 5.0 \times 10^{-7}\text{s}$  (CFL  $\approx 0.15$ ), up to  $1.0 \times 10^{-4}\text{s}$  (200 steps)

In this (nearly) pure water case for the entire computational domain, the cell-interfacial speed of sound used in flux functions is that of liquid, not the gas-liquid-averaged one. The results are shown in Fig. B1

From Figs. B1a and B1g, AUSM<sup>+</sup>-up (1, 1) and AUSM<sup>+</sup>-up (Niu) captured both the shock (right) and the expansion (left), albeit in a slightly diffused manner. Furthermore, AUSM<sup>+</sup>-up (Niu) needed a small timestep; otherwise, the computation blew up. On the other hand, AUSM<sup>+</sup>-up (0, 0), showed severe oscillations as in Fig. B1c. AUSM<sup>+</sup>-up (0.5, 0.5), showing sharp wave capturing in Fig. B1b, looked the best balance among AUSM<sup>+</sup>-up results. SLAU, SLAU2, and AUSM<sup>+</sup>-up2, in turn, bore only velocity oscillations of  $O(0.01)$  m/s, an order smaller than the local velocity  $O(0.1)$  m/s [or a Mach number order of  $O(10^{-4})$ ] (Figs. B1d-f). Although physically correct solutions were reportedly

obtained for low speed steady flows of  $M \approx O(10^{-3})$  by those flux functions as surveyed by Kitamura et al. in [26, 27, 35], it is possible that additional treatment may be required for transient, very low speed flows,  $M < O(10^{-4})$ . One of such remedies is enhancing pressure difference term in mass flux of SLAU and SLAU2, as recently suggested by Dr. Ashvin Hosangadi of Combustion Research and Flow Technology (CRAFT Tech), Inc., PA, USA, (in private communication through Dr. Eiji Shima, JAXA, Japan, on Feb. 29, 2012, and also in [36]). This is realized, for example, by replacing  $\chi$  with  $\chi/(1-\chi)$  and introducing cutoff Mach number,  $M_{co}$  ( $=0.05$  here), into Eq. (14f) as:

$$\widehat{M} = \min \left( 1.0, \max \left( \frac{1}{a_{1/2}} \sqrt{\frac{\mathbf{u}_{k,L}^2 + \mathbf{u}_{k,R}^2}{2}}, M_{co} \right) \right) \quad (\text{B.1})$$

Although such a correction sacrifices parameter-free nature of SLAU and SLAU2, its effect is confirmed from the result of SLAU2 with this very low Mach correction as included in Fig. B1h, in which the velocity oscillations were significantly reduced, but requiring a very small CFL number to maintain stability. Nevertheless, since only problems where such a small velocity error is almost negligible are solved, this very low Mach correction is not applied in the main text of the paper. For those flows, all the methods except for AUSM<sup>+</sup>-up (0, 0) and AUSMPW+, which showed divergence (and also showed possibility that the weighting function in this flux is not suitable for use in stiffened gas EOS), may be applied.

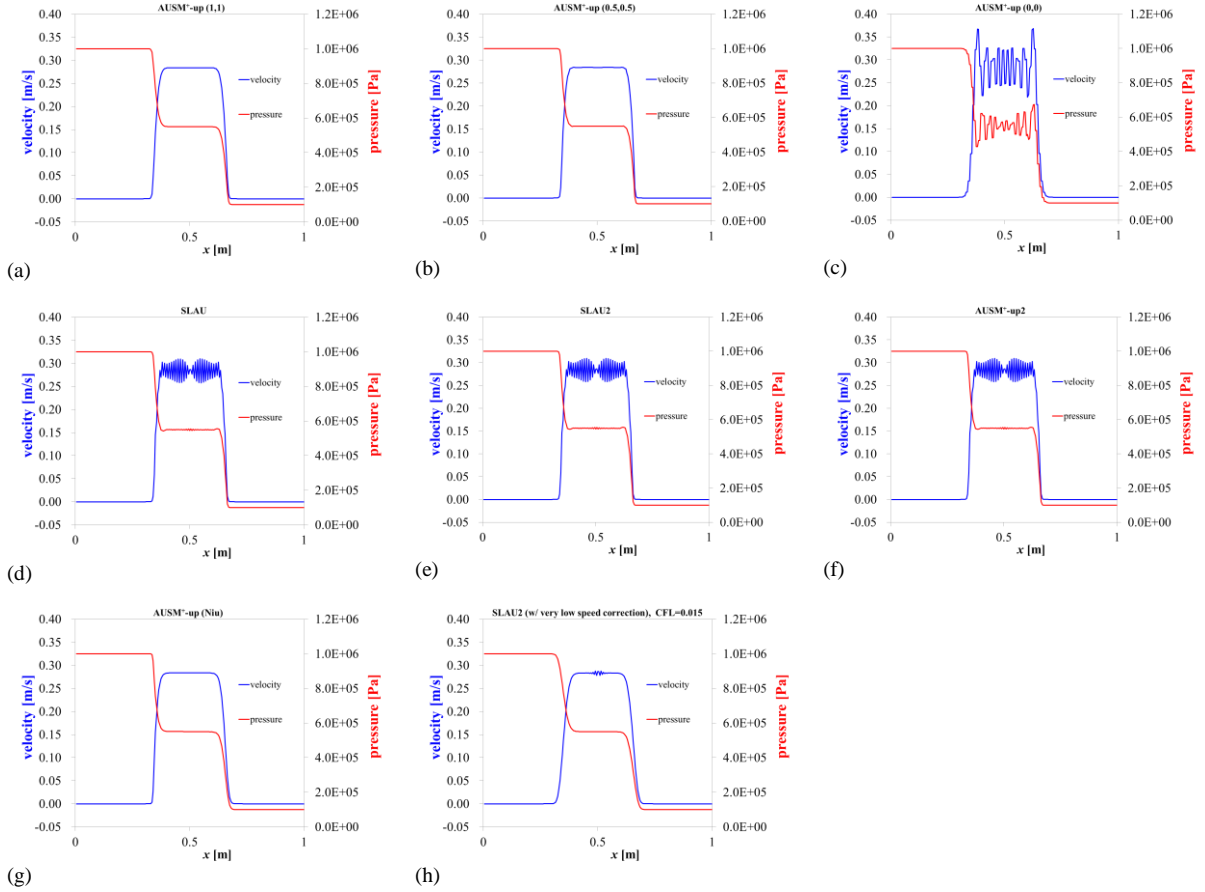


Figure B1: Underwater shock tube solutions at  $t=1.0 \times 10^{-4}$  s (a) AUSM<sup>+</sup>-up (1, 1); (b) AUSM<sup>+</sup>-up (0.5, 0.5); (c) AUSM<sup>+</sup>-up (0, 0); (d) SLAU; (e) SLAU2; (f) AUSM<sup>+</sup>-up2; (g) AUSM<sup>+</sup>-up (Niu); (h) SLAU2 (with very low Mach correction,  $M_{co}=0.05$ ) (10 times smaller time step; CFL $\approx$ 0.015).

## Appendix C: Combination with Exact Riemann Solver

We have basically followed the work by Liou et al. in [14], in which AUSM<sup>+</sup>-up, one of AUSM-family fluxes, was used standalone. In [13], on the other hand, Chang and Liou used AUSM<sup>+</sup>-up only at gas-gas and liquid-liquid interfaces, and the exact Riemann (Godunov) solver is used at phase

interfaces. We confirmed that the latter choice, although computationally more expensive, is able to deal with more challenging problems, such as water-air shock tube with high pressure ratio (PR),  $10^3$ , which will be briefly demonstrated below.

### C.1 Water-to-Air Shock Tube with High Pressure Ratio (Two-Fluid Flow)

Similarly to 3.3.2, the problem setup is given as follows, but with  $PR=10^3$  (which could not be treated by a single AUSM-family flux), as opposed to the original value of 2:

- $(p, \alpha_g, u_k, T_k)_L = (10^8 \text{ Pa}, \varepsilon, 100 \text{ m/s}, 0 \text{ m/s}, 308.15\text{K})$  for  $x \leq 5\text{m}$
- $(p, \alpha_g, u_k, T_k)_R = (10^5 \text{ Pa}, 1-\varepsilon, 100 \text{ m/s}, 0 \text{ m/s}, 308.15\text{K})$  for  $x > 5\text{m}$

where  $k=g, l$ , and  $\varepsilon=1.0 \times 10^{-5}$  ( $\varepsilon_{\min}=1.0 \times 10^{-7}$ ,  $\varepsilon_{\max}=1.0 \times 10^{-3}$ ), with the grid and time step:

- 500 cells:  $\Delta x=0.02\text{m}$ ,  $\Delta t=2.0 \times 10^{-6}\text{s}$  ( $CFL \approx 0.16$ ) for AUSM<sup>+</sup>-up(1,1)/Godunov;  $\Delta t=1.0 \times 10^{-6}\text{s}$  ( $CFL \approx 0.08$ ) for SLAU2/Godunov, up to  $2.0 \times 10^{-3}\text{s}$  (1,000 or 2,000 steps)

The results of AUSM<sup>+</sup>-up(1,1)/Godunov and SLAU2/Godunov are shown in Fig. C1 (pressure is displayed in log scale for better presentation). Both the results successfully captured expansion in water as steep pressure gradients and relatively weak shock in air without oscillations.

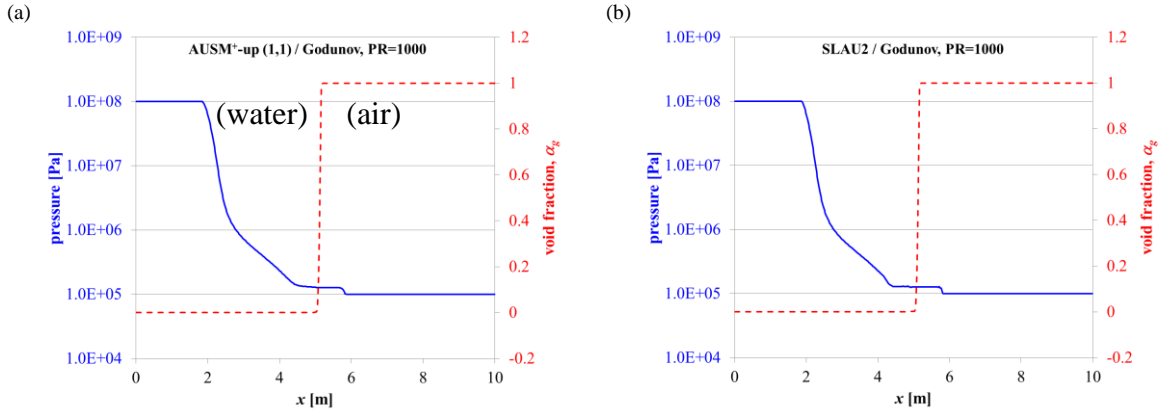


Figure C1: Water-to-Air Shock Tube Problem (with High Pressure Ratio,  $PR=1,000$ ) Solutions at  $t=2\text{ms}$ , (a) AUSM<sup>+</sup>-up (1, 1)/Godunov; (b) SLAU2/Godunov.

### C.2 Moving Phase Discontinuity (Two-Fluid Flow)

As in 3.1, the moving phase contact discontinuity was solved using AUSM<sup>+</sup>-up(1,1)/Godunov and SLAU2/Godunov. As shown in Fig. C2, the pressure was preserved across the phase interface within  $O(10^{-5})$  [Pa], as well as the AUSM<sup>+</sup>-up (1, 1) or SLAU2 alone.

Therefore, we have confirmed that while AUSM-family fluxes can solely be used in most cases, we can resort to the exact Riemann solver for problems involving high pressure ratio in combination with AUSM-family fluxes such as AUSM<sup>+</sup>-up (1, 1) or SLAU2. Further survey on both single AUSM-family and AUSM-family/Godunov methods is our next interest as an immediate future work.

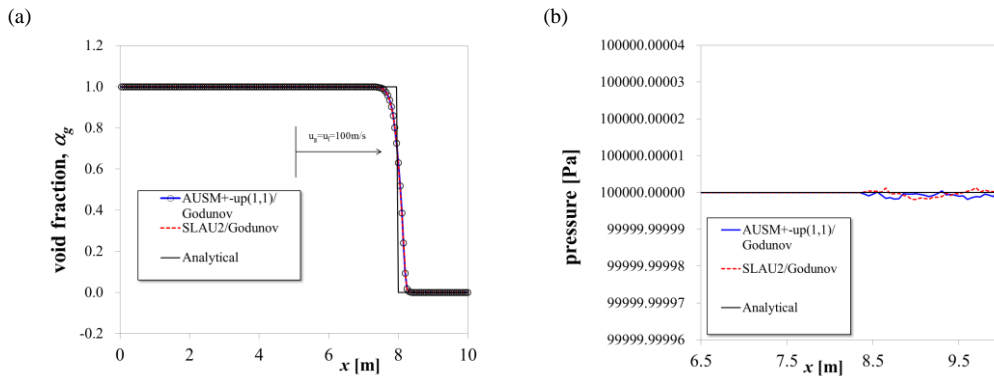


Figure C2: Moving Phase Contact Discontinuity Solutions (using Exact Riemann Solver at Phase Interface) at  $t=0.03\text{s}$  (a) Void fraction,  $\alpha_g$ ; (b) Pressure (expanded scale).